



## A review on micromechanical modelling of progressive failure in unidirectional fibre-reinforced composites

Lei Wan<sup>a,b</sup>, Yaser Ismail<sup>c</sup>, Yong Sheng<sup>d</sup>, Jianqiao Ye<sup>e</sup>, Dongmin Yang<sup>a,\*</sup>

<sup>a</sup> Institute for Materials and Processes, School of Engineering, University of Edinburgh, Edinburgh, EH9 3FB, UK

<sup>b</sup> Advanced Composites Research Group, School of Mechanical and Aerospace Engineering, Queen's University Belfast, Belfast, BT9 5AH, UK

<sup>c</sup> Groundforce Shorco, Gildersome, Leeds LS27 7HJ, UK

<sup>d</sup> School of Computer Science, University of Hull, Hull, HU6 7TQ, UK

<sup>e</sup> School of Engineering, Lancaster University, Lancaster, LA1 4YW, UK

### ARTICLE INFO

#### Keywords:

Fibre reinforced polymer composite (FRP)  
Finite element method (FEM)  
Discrete element method (DEM)  
Progressive failure  
Multiaxial loadings

### ABSTRACT

The recent decades have seen various attempts at the numerical modelling of fibre-reinforced polymer (FRP) composites in the aerospace, auto and marine sectors due to their excellent mechanical properties. However, it is still challenging to accurately predict the failure of the composites because of their anisotropic and inhomogeneous characteristics, multiple failure modes and their interaction, especially under multiaxial loading conditions. Micromechanics-based numerical models, such as representative volume elements (RVEs), were developed to understand the progressive failure mechanisms of composites, and assessing existing failure criteria. To this aim, this review paper summarises the development of micromechanics-based RVE modelling of unidirectional (UD) FRP composites reported in the literature, with a focus on those models developed using finite element (FE) and discrete element (DE) methods. The generation of fibre spatial distribution, constitutive models of material constituents as well as periodic boundary conditions are briefly introduced. The progressive failure mechanisms of UD FRP composites simulated by RVEs under various loadings are discussed and the comparison of failure envelopes predicted by numerical results and classical failure criteria are reviewed.

### 1. Introduction

Carbon fibre-reinforced polymer (CFRP) and glass fibre-reinforced polymer (GFRP) composites are widely used in the aerospace, transportation and energy fields due to their excellent mechanical properties such as high strength-to-weight and modulus-to-weight ratios, enhanced corrosion, heat resistance and superior thermal stability. However, due to the complex nature of composites and progressive failure characteristics, a complete and fully validated theory is still needed for the failure prediction of composite materials, especially under multiaxial loading conditions.

Five microscopic main failure modes, namely fibre breakage, fibre pull-out, fibre/matrix debonding, matrix cracking and delamination are all captured in Fig. 1, which is an SEM image of a cross-section of cross-ply CFRP composite. Fibre breakage usually occurs when the stress acting on the fibre is beyond its strength, and it can be accumulated within the composite laminates during the loading process. Generally, the strength of fibres varies due to the fact of randomly distributed flaws along each fibre, and Weibull distribution is usually used to represent the fibre strength statistically. Fibre/matrix interfacial debonding

often occurs either due to the high shear stress concentration as a result of fibre breakage, or high tensile stress, which is perpendicular to the fibre direction. Matrix cracking is normally induced by defects or high tensile/shear stress under different loading conditions as well as some other damages like fibre breakage or interfacial debonding. Delamination can be initiated by the shear stress between two adjacent layers under impact or compression loadings. Delamination is a critical damage mode which can cause significant stiffness and strength reduction of composite structures, leading to final catastrophic failure or even fracture of the whole structure [1].

In laminated UD FRP composites, the damage is normally initiated from matrix cracking or interface debonding at the micro-scale or constituent level, and propagates in the matrix and/or interface, which can be detected at the meso-scale or lamina level. The instantaneous and catastrophic failure of the composite structure occurs at the macro-scale or laminate level as soon as the threshold of fibre is reached. The entire failure process covers three different stages, ranging from micro-scale, meso-scale to macro-scale levels, each of which has been researched and different failure mechanisms are investigated at a specific level [2].

\* Corresponding author.

E-mail address: [Dongmin.Yang@ed.ac.uk](mailto:Dongmin.Yang@ed.ac.uk) (D. Yang).

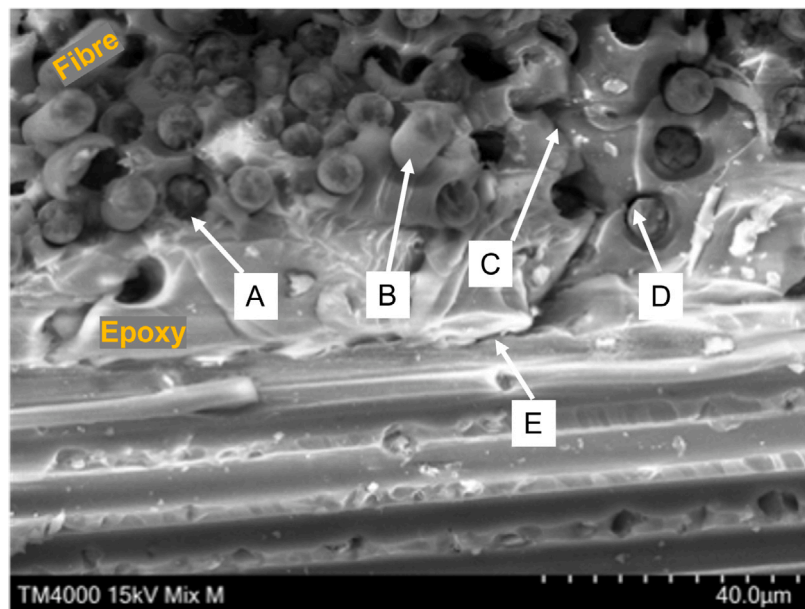


Fig. 1. Main different failure modes of composite material: (A) fibre breakage; (B) fibre pull-out; (C) brittle fracture of an epoxy matrix, (D) fibre/matrix debonding and (E) delamination.

The interaction between damages at different length scales needs to be fully understood to provide a more reliable and valid prediction of failure in laminates. The analytical estimation of the mechanical properties of FRP composites is a non-trivial problem even for a linear-elastic composite part with relatively simple microstructure [3]. The generalisation of the analytical estimations on complex microstructure and nonlinearity of material behaviour presents an even bigger challenge for researchers. Experimental studies can provide realistic validations for the failure predictions obtained from analytical models and numerical models. Currently, the application of non-destructive evaluation techniques, such as synchrotron radiation computed tomography (SRCT), digital image correlation (DIC) and Acoustic emission (AE), in the measurement of damage initiation and propagation enables researchers to detect in-situ damage at the different length scales, greatly promoting the understanding of damage occurring in the composite. However, some of these advanced techniques are difficult and expensive to access, especially for the failure prediction of composites under multiaxial loadings due to the limitations of the apparatus. Moreover, the input parameters of these aforementioned analytical models are obtained through costly and time-consuming experiments for different material systems. The results obtained from a given UD FRP composite material system cannot be extrapolated to other configurations with different fibre volume fractions or constituent properties, leading to a huge amount of investment in their physical characterisation [4].

With the rapid development of computing power, numerical methods (i.e. finite element methods (FEM) and discrete element methods (DEM)) have become a very useful tool to conduct the micromechanical analysis for composite materials, especially high-fidelity numerical modelling is widely used in the failure prediction of composites in last two decades due to its capability of providing more details about the damage initiation and propagation in the composite when complex loadings such as biaxial or triaxial stresses are applied. Heidari-Rarani et al. [5] conducted a brief review on micromechanical analysis of UD FRP composites with various methods and compared their capabilities for predicting the elastic properties. However, to the authors' best knowledge, there is no comprehensive review on the failure analysis of composites based on micromechanical modelling, especially under multiaxial loadings. This review aims to provide a detailed review of the construction of representative volume elements within the framework of micromechanical modelling, covering the spatial distribution

of fibres embedded in a matrix, constitutive models of material constituents, periodic boundary conditions and failure analysis of UD FRP composites under various loadings with FEM and DEM.

## 2. Microscale modelling of progressive failure in UD FRP composites with FEM

Computational micromechanics offers a novel approach for a better understanding of the deformation and fracture mechanisms by means of the representative volume element (RVE) modelling, in which the mechanical properties of the constituents can be obtained from the experiments. An RVE has the smallest volume size to maintain the computational cost, but is large enough to contain microscopic necessary information (i.e. volume fraction, constituent information, fibre distribution) of a composite. Compared to the classic homogenisation techniques, computational micromechanics presents two main advantages. On the one hand, it takes the influences of the geometry and spatial distribution of the three phases into consideration, such as the size or shape of the fibre, clustering, and the interface connectivity between fibre and matrix. On the other hand, the details of the stress and strain distributions under different loading conditions can be captured, leading to a more accurate estimation of the onset of damage and its progression as well as the prediction of the final failure strength [6].

In this section, progressive failure analysis of UD FRP composites based on micromechanical modelling is reviewed, with a focus on the RVE modelling in combination with FEM. Three approaches, namely experimental, coupled experimental–numerical and numerical ones, are compared for the generation of randomly distributed fibres within RVEs. The constitutive models of constituents (i.e. fibres, matrix and fibre/matrix interface) are discussed, in which the fundamentals of four different models for matrix behaviours are briefly recovered. The selection of the constitutive model for the matrix is compared under uniaxial and multiaxial loadings. In addition, periodic boundary conditions and the approach to applying multiaxial loadings are briefly discussed. Progressive failure analysis of UD FRP composites under various uniaxial loadings, considering five main failure modes including fibre tensile failure, fibre kinking, matrix cracking, matrix yielding and fibre/matrix interface debonding, are discussed in detail.

## 2.1. Generation of fibre distribution

The ideal approach to generate the random fibre distribution is to obtain the spatial fibre position from the realistic experimental scanning electronic microscopic (SEM) image directly, in which the fibre centroids can be located by the colour of the fibres [7]. Vaughan and McCarthy used a combined experimental–numerical approach to generate the statistically equivalent random fibre distributions for composite materials [8]. The fibre volume fraction, fibre diameter and its statistical distributions were characterised experimentally and the nearest neighbour algorithm (NNA) was used to define the inter-fibre distances based on experimental measurements. The advantage of the image-based method lies in the smallest discrepancy between the generated microstructure and the original cross-section of the composite material. However, this task is a time-consuming and special requirement of computer software for the processing of experimentally obtained images.

In order to generate the random distribution of fibres efficiently, several numerical models were proposed to generate statistically equivalent RVEs of composite materials. A hard-core model, also called the random sequential absorption model, was widely used for the generation of RVE models, in which the fibres are represented by discs randomly distributed in a specific square domain without overlaps. However, it is difficult for this simple model to generate randomly distributed fibres with a volume fraction higher than 50% due to a jamming limit [9]. This problem was later tackled with an initially periodic shaking model (IPSM) by shaking an initial hexagonal packing of the fibres [10]. Melro et al. [11] developed a hard-core shaking model (HCSM) to achieve fibre volume fractions higher than 50%, in which the aforementioned hard-core model was used to generate the initial fibre distribution and random motion of fibres was triggered by an arbitrary displacement on fibres. This algorithm provides users with a high level of control with several input variables. On the other hand, a simpler algorithm, called random sequential expansion (RSE), was developed by Yang et al. [12] to control the inter-fibre distances. However, a uniform diameter of fibres was assumed and some inter-fibre distances were set as zero in order to achieve the volume fraction of 68% which could cause numerical difficulties. Yaser et al. [13] proposed a novel approach based on the discrete element method to generate a random distribution of long-fibre with high volume fractions (such as 60%, 65% and 68%) and any specified inter-fibre distances. Various fibre diameters extracted from the experimental measurement were assigned in order to achieve the random distribution of fibres.

Fig. 2 shows the comparison of the approaches to generating random fibre distributions using experimental, experimental–numerical and numerical methods. Fig. 2(a–c) represent the procedure of generating random fibre distribution purely from the experimental SEM image. As shown in Fig. 2b, the obtained non-periodicity of fibre distribution at the edges is converted to a periodic microstructure by generating corresponding parts at the opposite edge ( $B1'$ ,  $B2'$ ,  $T1'$ ) based on the fibre position at the edge ( $B1$ ,  $B2$ ,  $T1$ ) obtained from the experiment. Thus, the geometrical CAD model can be generated, see Fig. 2(c). Fig. 2(d–f) illustrate the procedure of generating random fibre distributions using the nearest neighbour algorithm. A random point is created with a coordinate  $(x_1, y_1)$  and the diameter of the surrounding fibre is drawn from a lognormal distribution fitting the experimentally measured diameter distribution. A created second point  $(x_2, y_2)$  is the centre of the second nearest neighbour of the first fibre and its distance is assigned from the adjusted first nearest neighbour distribution function with a random angle of  $\theta_1$ . The same happens to generate the third point  $(x_3, y_3)$ . For any fibre crossing a boundary, a corresponding fibre is placed on the opposing boundary to maintain geometric periodicity. Fig. 2(g–i) represent the procedure of generating random fibre distribution by adding extra discs into the original numerical model and applying periodic boundary conditions. Fibres are initially placed in a regular cubic arrangement (Fig. 2g). Extra

fibres/discs are added in random places and overlap with others to achieve the target volume fraction (Fig. 2h). A random velocity is applied simultaneously to each of the discs that move in a way similar to the Brownian motion, which is governed by the Newton's Second Law and the collisions between any two discs are according to the Hertz contact law [14].

## 2.2. Constitutive modelling of composite constituents

### 2.2.1. Constitutive model of fibres

In the micromechanics-based modelling, the carbon fibres are usually modelled as linearly elastic, transversely isotropic solids under transverse and/or shear-dominated loadings [4,15,16]. While in the longitudinal tension, the fibres are modelled as isotropic and linear-elastic up to failure. In order to capture the stochastic failure of fibres under longitudinal tension, two strategies are usually used: synthetically insert the fracture planes perpendicular to the fibre direction using a cohesive surface with experimentally-obtained stochastic failure parameters [17], and assign the statistically analysed (i.e. Weibull distribution [18]) stochastic failure strength to fibres with a thermodynamically consistent isotropic damage model [19,20]. In longitudinal compression, the fibres are either modelled as transversely isotropic and linear-elastic [21] and a damage model (i.e. a continuum damage mechanics model [22], maximum stress/strain failure criteria [23,24]) to capture brittle failure. However, a distinct nonlinearity is observed on the stress–strain curves from single-fibre tests on AS4 carbon fibres under longitudinal loadings [25]. It was found that if the mechanical response of the fibres is assumed to be linear, the stress prediction under longitudinal tension will not result in remarkable errors, but compressive stresses will be overpredicted, especially under high compressive strains. Such nonlinear elastic response of the fibres was represented by an analytical model with a single nonlinear parameter [26], which has not been implemented into micromechanical modelling.

### 2.2.2. Constitutive model of matrix

The polymeric matrix is usually modelled as an isotropic elasto-plastic solid. It has been found that the mechanical behaviour of polymer is sensitive to the hydrostatic stress [27], and exhibits a completely different behaviour when subjected to various simple uniaxial loading conditions, such as brittle in tension while plastic in compression and shear. These characteristics of polymers are considered in the failure analysis of composite materials under multiaxial stress states, by means of the Mohr–Coulomb (M–C) yielding criterion [15], the extended Drucker–Prager (D–P) yield model [28] associated with a ductile damage criterion [29], the modified Drucker–Prager plastic damage model [30–32] and the elasto-plastic with isotropic damage constitutive model, proposed by Melro et al. [33]. Here these four widely used constitutive models of a matrix are briefly recalled below and listed in Table 1.

The Mohr–Coulomb yielding criterion states that yielding will occur on a given plane when the shear stress  $\tau$  exceeds the sum of cohesion yielding stress  $c$  and the friction force acting along the failure plane, such that  $\tau = c - \sigma_n \tan \Phi$ , in which the  $\Phi$  is the internal friction angle. For the M–C model, the  $c$  and  $\Phi$  can be expressed with the tensile and compressive strengths of the material as  $\sigma_t = 2c \frac{\cos \Phi}{1 + \sin \Phi}$  and  $\sigma_c = 2c \frac{\cos \Phi}{1 - \sin \Phi}$ . A non-associative flow rule is usually used to compute the direction of plastic flow, in which the flow potential was proposed by Menetrey and William [34].

In order to take into account the progressive failure behaviour of matrix, the extended linear D–P yield criterion and the ductile damage criterion are used to model the plastic deformation and the progressive damage process. The extended linear D–P criterion can be expressed as below [30]:

$$F = t - p \tan \beta - d = 0, t = \frac{1}{2} q \left[ 1 + \frac{1}{k} - \left( 1 - \frac{1}{k} \right) \left( \frac{r}{q} \right)^3 \right] \quad (1)$$

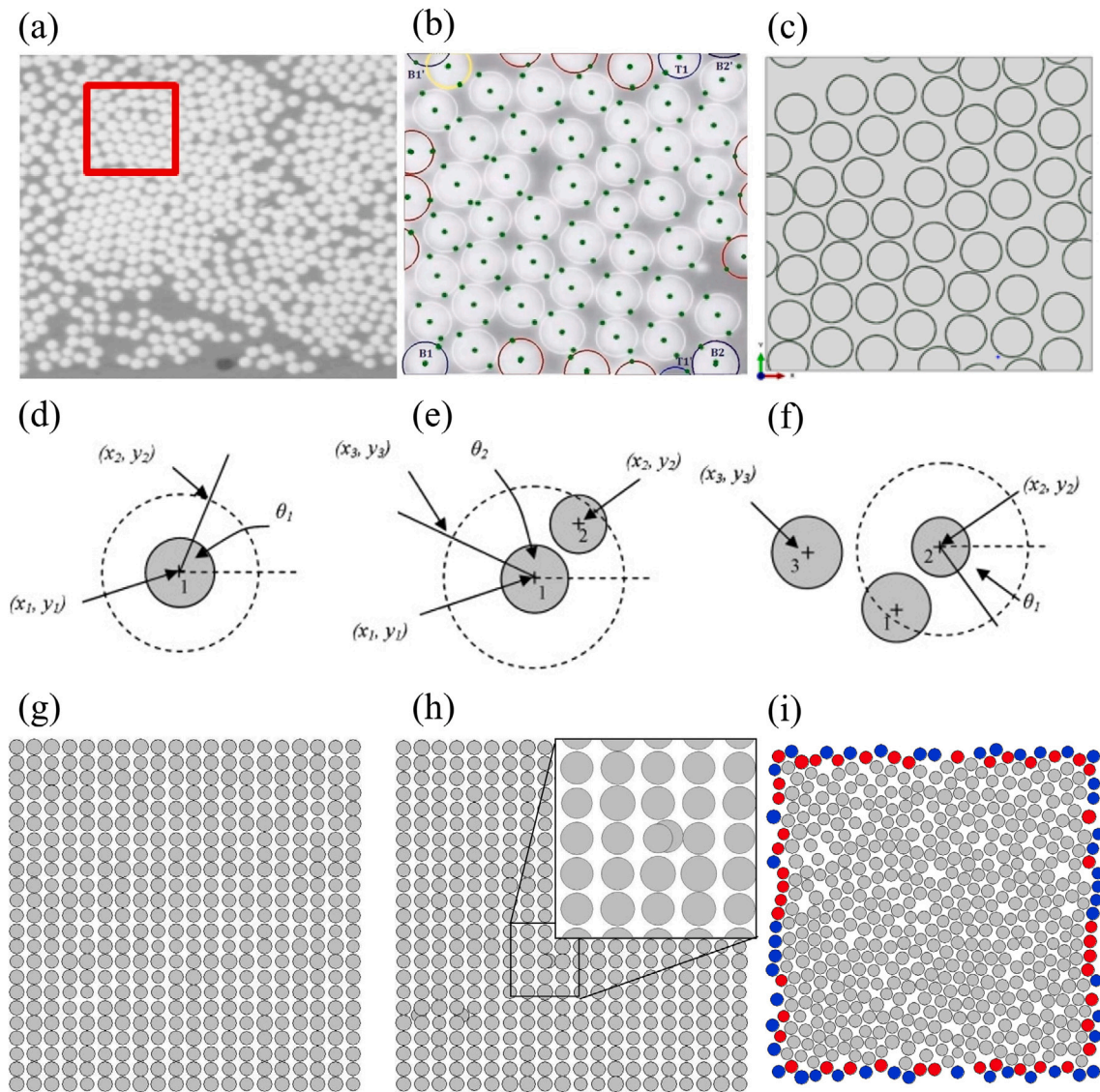


**Fig. 2.** Comparison of the generation of random fibre distributions using experimental approach (a–c) [7], experimental–numerical approach (d–f) [8] and numerical approach (g–i) [13]. ((a) is the SEM image of a cross-section of UD CFRP composites, a representative cross-section was cut from (a) in the red square and the fibre position was determined by its origin and two points on the circle, see (b). Red circles on the edges represent the periodicity on the opposite edges, and blue circles represent mean there is no periodicity on the opposite edges which needs some adjustments. (c) is the geometrical model after adjustment. (d–f) illustrate the nearest neighbour algorithm. (g–i) represent the procedure of generating random fibre distribution by adding extra discs into the original numerical model and applying periodic boundary conditions. In (f), the grey discs stay within the RVE while the red and blue ones are moving across the RVE boundaries to maintain a certain fibre fraction volume.). (For interpretation of the references to colour in this figure legend, the reader is referred to the web version of this article.)

where  $p$  is the equivalent pressure stress,  $\beta$  is the slope of the linear yield surface in the  $p - t$  plane,  $d$  is the cohesion of the material ( $d \neq c$ ) and related to the yielding stress when the yielding behaviour is defined by the uniaxial compression, tension and shear,  $q$  is the Mises equivalent stress,  $k$  is the ratio of the yield stress in triaxial tension to the yield stress in triaxial compression, which controls the difference in yielding behaviour between tension and compression. According to the relation between the M–C model and the D–P model, the internal friction angle  $\Phi$  and cohesion yielding stress in the M–C model can be converted to the  $\beta$  and  $d$  in the case of plain strain using [30]:

$$\tan\beta = \frac{3 \sin \Phi}{\sqrt{3 + \sin^2 \Phi}}, \quad \frac{d}{c} = \frac{3 \cos \Phi}{\sqrt{3 + \sin^2 \Phi}} \quad (2)$$

The plastic flow of the material is controlled by the flow potential  $G$ , and is expressed as

$$G = t - p \tan \psi \quad (3)$$

where  $\psi$  is the dilation angle in the  $p - t$  plane. Experimental findings [35] showed that the use of the associated flow rule for polymers overestimates the extent of plastic dilatancy, thus a non-associated flow rule is more suitable for computing the direction of the plastic flow.

Experimental findings [27] showed that the polymer exhibits a rather brittle fracture behaviour under the uniaxial tension while a large plastic deformation under uniaxial compression and pure shear. The damage behaviour can be governed by the ductile damage criterion, which assumes that the equivalent plastic strain at the onset of damage,  $\bar{\epsilon}_D^{pl}$  is a function of stress triaxiality  $\eta$  and strain rate  $\dot{\bar{\epsilon}}^{pl}$ , where  $\eta = -p/q$ . The damage propagation is controlled by a damage evolution law, in which the softening behaviour is characterised by a stress–displacement response to alleviate mesh dependency of results. This can be achieved in the finite element model by introducing the critical fracture energy using the crack band model [36], defined as the energy required to open a unit area of the crack, and a characteristic

length  $l_{ch}$ . The fracture energy can be expressed as:

$$G_f = \int_{\bar{\epsilon}_0^{pl}}^{\bar{\epsilon}_f^{pl}} l_{ch} \sigma_y d\bar{\epsilon}_f^{pl} = \int_0^{\bar{u}_f^{pl}} \sigma_y d\bar{u}^{pl} \quad (4)$$

where  $\bar{\epsilon}_0^{pl}$  and  $\bar{\epsilon}_f^{pl}$  are the equivalent plastic strain at the damage onset and failure, respectively. The equivalent plastic displacement at failure is defined as  $\bar{u}_f^{pl} = 2G_f/\sigma_{y0}$ . More details about the damage model and the numerical implementation can be found in [30,37].

Alternatively, a continuum plasticity-damage model based on D-P model was developed by Lubliner et al. [31] and modified by Lee and Fenves [32]. The yielding surface is expressed by a modified D-P yielding function as:

$$\Phi(I_1, J_2, \sigma_1, \beta', \alpha) = \frac{1}{1-\alpha} \left( \sqrt{\frac{3J_2}{2}} + \frac{I_1}{3} \alpha + \beta' \langle \sigma_1 \rangle \right) - \sigma_{yc} = 0 \quad (5)$$

where  $I_1$  stands for the first invariant of the stress tensor,  $J_2$  is the second invariant of the deviatoric stress tensor,  $\alpha$  is the pressure-sensitivity parameter of the Drucker-Prager yield criterion,  $\sigma_1$  is the maximum principal stress,  $\langle \cdot \rangle$  is the Macaulay brackets (which return the argument if positive and zero otherwise) and  $\beta'$  is a parameter function of the yield stresses under tension  $\sigma_{yt}$  and  $\sigma_{yc}$ ,

$$\beta' = \frac{\sigma_{yc}}{\sigma_{yt}} (1 - \alpha) - (1 + \alpha) \quad (6)$$

The brittle behaviour in tension is taken into account by means of a linear softening law, while the considerable plastic deformation at constant flow stress, which occurs in compression and shear after yielding, can lead to final failure by the formation of a shear band. Mesh sensitivity problems are tackled with the crack band model [36] using Eq. (4).

Unlike the Mohr-Coulomb and Drucker-Prager yielding criteria, the one proposed in [33] appears to be more attractive due to its mathematical formulation, which contains no geometrical features such as edges or vertices on its smooth yielding surface [38], resulting in a more convenient implementation of this constitutive model.

The paraboloidal yielding criterion, originally proposed by [39] reads

$$\Phi(\sigma, \sigma_{yt}, \sigma_{yc}) = 6J_2 + 2I_1(\sigma_{yc} - \sigma_{yt}) - 2\sigma_{yt}\sigma_{yc} \quad (7)$$

where  $J_2$  is the second invariant of the deviatoric stress tensor,  $I_1$  is the first invariant of the stress tensor.  $\sigma_{yt}$  and  $\sigma_{yc}$  are the yielding strengths under tension and compression, respectively. A non-associative flow rule is used to correct the definition of the volumetric deformation in plasticity:

$$g = \sigma_{vm}^2 + \alpha p^2 \quad (8)$$

where  $\sigma_{vm} = \sqrt{3J_2}$  is the von Mises equivalent stress,  $p = 1/3I_1$  is the hydrostatic pressure and  $\alpha$  is a material parameter for the correct definition of the volumetric component of the plastic flow, which is given as

$$\alpha = \frac{9(1 - 2\nu_p)}{2(1 + \nu_p)} \quad (9)$$

where  $\nu_p$  is the plastic Poisson's ratio and the  $\alpha$  can be uniquely defined if the  $\nu_p$  is determined in a standard tension test. The flow rule is given by the flow potential in Eq. (8), which reads

$$\dot{\epsilon} = \dot{\gamma} \frac{\partial g}{\partial \epsilon} \quad (10)$$

where the parameter  $\dot{\gamma}$  is the time derivative of the plastic multiplier that should be consistent with the classical loading/unloading conditions:

$$\dot{\gamma} \geq 0, \Phi \leq 0, \dot{\gamma}\Phi = 0. \quad (11)$$

In order to mitigate the mesh dependence on material softening, the crack band model [36] is utilised for the implementation of the damage

evolution law. A thermodynamically consistent isotropic damage model is used, in which the damage activation function reads

$$\frac{3\hat{J}_2}{\sigma_{ft}\sigma_{fc}} + \frac{\hat{I}_1(\sigma_{fc} - \sigma_{ft})}{\sigma_{ft}\sigma_{fc}} - 1 = 0 \quad (12)$$

where  $\sigma_{ft}$  and  $\sigma_{fc}$  are the tensile and compressive strengths of the matrix, while the invariants  $\hat{I}_1$  and  $\hat{J}_2$  are determined using the undamaged stiffness tensor.

The exponential damage evolution law, which is denoted with the damage variable  $d_m$ , is given by:

$$d_m = 1 - \frac{e^{A_m(3 - \sqrt{7 + 2r_m^2})}}{\sqrt{7 + 2r_m^2} - 2} \quad (13)$$

where  $A_m$  is the parameter responsible for the energy release rate, related to the characteristic length and the  $r_m$  is the damage internal variable. The detailed constitutive model and its numerical implementation can be found in [33].

### 2.2.3. Constitutive model of fibre/matrix interface

It was experimentally observed that the shear strength increases in UD composite laminae under moderate transverse compressive stress when subjected to biaxial loads [40], compared to pure shear stresses. This is difficult to be captured adequately with the current built-in cohesive zone element in ABAQUS [30] since when modelling with the conventional cohesive element, the friction can only be considered when the cohesive element is totally damaged and removed from the finite element mesh. This phenomenon was also theoretically predicted by Puck's failure theory and numerically simulated with a cohesive surface together with a pure Coulomb model [4] or a cohesive-friction damage approach implemented into ABAQUS via a VUMAT subroutine [7,41,42].

During the RVE modelling with the finite element method, the interface modelling is a very crucial part of the model, usually in which a cohesive crack model is implemented to simulate the mechanical response of the interface between the fibre and matrix. In the linear behaviour before the onset of damage, an initial stiffness  $K_i$  ( $10^5$  GPa/mm) is used in most research [16,43-46] to simulate the elastic behaviour of the RVE model, which is a numerical parameter large enough to ensure the displacement continuity at the interface and to avoid any modification of the stress fields around the fibre before damage [46]. However, it was found that the average Young's modulus and strength of the interphase are around 5 and 9 times larger than those of the bulk resin matrix [44], and the interphase was modelled as a separate zone with the same constitutive and damage model but different mechanical properties from the matrix, which makes the model more complicated. Therefore, the parameter identification of the interphase of the carbon fibre-reinforced composite was conducted by the inverse strategy based on the experimental data, microstructural modelling method and Kriging metamodel [47] and artificial neural networks [48], including the identification of thickness, normal and shear stiffnesses of fibre/matrix interface and transverse stiffness of fibres, which are challenge to be determined experimentally. These sets of parameters was applied to predict the elastic and strength properties of CFRP composite yarn [49] and failure analysis of CFRP composites under multiaxial loadings [50,51].

The fibre/matrix interface is modelled using a cohesive element, which is controlled by the bilinear traction-separation law. The elastic behaviour is written in terms of an elastic constitutive matrix that relates the nominal stresses to the nominal strains across the interface. The nominal traction stress vector  $t$  consists of three components:  $t_n$ ,  $t_s$ ,  $t_t$ , which represent the normal and two shear tractions, respectively. The corresponding separations are denoted by  $\delta_n$ ,  $\delta_s$  and  $\delta_t$ , and the original thickness of the cohesive element is denoted by  $T_0$ , then the nominal strains can be defined as

$$\epsilon_n = \frac{\delta_n}{T_0}, \epsilon_s = \frac{\delta_s}{T_0}, \epsilon_t = \frac{\delta_t}{T_0} \quad (14)$$

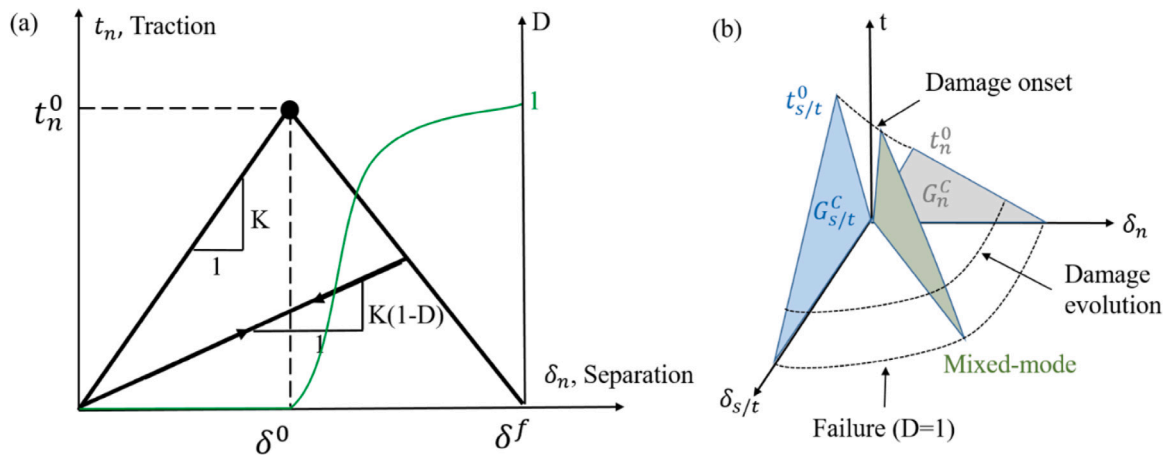


Fig. 3. Schematic of the traction–separation cohesive law of the interface: (a) uniaxial tension in the normal direction associated with the damage parameter ( $K$  is the initial stiffness in the normal direction,  $D$  is the damage parameter,  $t_n^0$  is the peak traction at the separation of  $\delta^0$  and  $\delta^f$  is the ultimate separation at failure. The green line represents the damage variable which increases from 0 at  $\delta^0$  and reaches 1 at  $\delta^f$ ) and (b) representation of mixed-mode damage evolution. (The grey and light blue triangles represent the single mode of the cohesive zone model while the olive green triangle in the middle represents the mixed mode of the cohesive model). (For interpretation of the references to colour in this figure legend, the reader is referred to the web version of this article.)

therefore, the elastic behaviour for the cohesive element can be written in Eq. (15). For simplicity of computation, uncoupled behaviour between the normal and shear components is desired so the off-diagonal terms in the elasticity matrix are set to be zero and the stiffness in two shear directions is assumed to be equal.

$$t = \begin{Bmatrix} t_n \\ t_s \\ t_t \end{Bmatrix} = \begin{bmatrix} K_{nn} & K_{ns} & K_{nt} \\ K_{ns} & K_{ss} & K_{st} \\ K_{nt} & K_{st} & K_{tt} \end{bmatrix} \begin{Bmatrix} \delta_n \\ \delta_s \\ \delta_t \end{Bmatrix} = \mathbf{K} \delta \quad (15)$$

Damage is initiated when a quadratic interaction function involving the nominal stress ratios reaches a value of one. This criterion can be represented as:

$$\left\langle \frac{t_n}{t_n^0} \right\rangle^2 + \left\langle \frac{t_s}{t_s^0} \right\rangle^2 + \left\langle \frac{t_t}{t_t^0} \right\rangle^2 = 1 \quad (16)$$

where  $\langle \cdot \rangle$  is the Macaulay brackets, which return the argument if positive and zero otherwise, and the bracket is also used to signify that a pure compressive deformation or stress state does not initiate damage.  $t_n^0$ ,  $t_s^0$ ,  $t_t^0$  represent the peak values of the nominal stress when the deformation is purely normal to the interface and purely in the first and second shear directions, respectively. Damage evolution is defined based on the dissipated fracture energy during the damage propagation. Once the damage initiates, the traction stress  $t^0$  is reduced depending on the interfacial damage parameter, which monotonically evolves from 0 (in absence of damage  $\delta^0$ ) to 1 (at the final failure  $\delta^f$ ), as shown in Fig. 3. The energy-based Benzeggagh–Kenane (BK law) damage propagation criterion [52] is adopted during the damage evolution of the cohesive elements, which is illustrated below:

$$G_n^C + (G_s^C - G_n^C) \left\{ \frac{G_s}{G_T} \right\}^\eta = G^C, G_s = G_s + G_t, G_T = G_n + G_s \quad (17)$$

where  $G_n^C$ ,  $G_s^C$  and  $G_t^C$  refer to the critical fracture energies required to cause failure in the normal, the first, and the second shear directions, respectively. Here  $G_s^C = G_t^C$  is set and  $G^C$  is the critical total interfacial fracture energy and the  $\eta$  is a cohesive property parameter. The published interface models and material properties for different FRP systems are summarised in Table 2.

### 2.3. Periodic boundary conditions

Periodic Boundary Condition (PBC) is imposed on the corresponding surfaces of the RVE by means of introducing the equations between the periodic nodes, in order to guarantee the periodicity of the displacement and traction fields as well as to ensure the continuity between

the neighbouring RVEs. The unified periodic boundary conditions are expressed in terms of the displacement vectors  $\vec{U}_1$ ,  $\vec{U}_2$  and  $\vec{U}_3$  which are related to the displacements between the opposite surfaces:

$$\begin{cases} \vec{u}(0, x_2, x_3) - \vec{u}(L_1, x_2, x_3) = \vec{U}_1 \\ \vec{u}(x_1, 0, x_3) - \vec{u}(x_1, L_2, x_3) = \vec{U}_2 \\ \vec{u}(x_1, x_2, 0) - \vec{u}(x_1, x_2, L_3) = \vec{U}_3 \end{cases} \quad (18)$$

where  $L_1$ ,  $L_2$  and  $L_3$  are the lengths of the RVE along with three orthogonal directions, respectively. The absolute formation is used to impose the linear constraint functions on the nodes at parallel opposite pairs of faces, and the edges and the vertices are extracted from the face to which they belong for the equations. The dummy nodes are introduced as reference points to apply the load in three directions, and then different loading conditions can be achieved by applying the displacement loads on the dummy nodes. When a displacement component of the dummy node is set free, this displacement can be computed by the FE solver under stress-free conditions. Therefore, the Poisson effect is permitted in a specific direction. For the uniaxial loading conditions, the load is applied to the axial direction, and then the axial components in the other two directions are set free for the consideration of the Poisson effects. While for combined transverse loading and in-plane shear, see Fig. 4(a), the loading is imposed with  $\vec{U}_2 = (\delta_s, \pm\delta, 0)$ , where the  $\pm\delta$  and  $\delta_s$  represent the transverse tension/compression and shear displacements, respectively. Same as the uniaxial loading conditions, the axial components in the other two directions are set free. When more complex loadings are taken into account, such as transverse, out-of-plane tension/compression and in-plane shear, see Fig. 4(b), an extra force should be imposed with  $\vec{F}_3 = (0, 0, \pm F)$ . More details about the implication of the PBC on the RVE are found in [66]. Three dummy nodes on three principal axes are introduced to apply loads and the origin of the RVE is fixed to avoid rigid body motion. The imposed strains were computed from the imposed displacements divided by the corresponding lengths, while the predicted normal and shear stresses were computed from the resultant normal and tangential forces acting on the RVE faces divided by the cross-sectional area.

### 2.4. Failure prediction of FRP composites under uniaxial loadings

The mechanical properties of fibres, matrix and fibre/matrix interface as well as fibre arrangement was found to have significant effects on the failure strength of composites under different loading conditions. Failure initiation in the matrix of composite materials under transverse tension was studied by Asp et al. [67,68]. Square, hexagonal

**Table 1**  
Comparison of published polymer models and material properties for micromechanics-based modelling.

|                                | Plastic model                 | Damage model                             | Uniaxial loadings | Multiaxial loadings |
|--------------------------------|-------------------------------|--|-------------------|---------------------|
| M-C                            | M-C yielding criterion        | –  | [15,53–55]        | [56]                |
| D-P & Ductile damage criterion | D-P yielding criterion        | Ductile damage initiation criterion [30] | [37,57]           | [58]                |
| D-P plastic damage model       | D-P yielding criterion        | Continuum damage model [31,32]           | [4,21,59,60]      | [4,50,51]           |
| Melro et al. [33] model        | A paraboloidal criterion [61] | Isotropic damage model                   | [20,43,62]        | [43,44,63]          |

**Table 2**  
Comparison of published interface models and material properties.

|            | Material system   | Interface modelling | Stiffness ( $k_n/k_s$ , GPa/m)      | Strength ( $\sigma_n/\tau$ , MPa) | Fracture energy ( $G_n/G_s$ , J/m <sup>2</sup> ) |
|------------|-------------------|---------------------|-------------------------------------|-----------------------------------|--|
| [53]       | HTA/6376          | Cohesive element    | $3.64 \times 10^9/1.4 \times 10^9$  | 85/125                            | 10/25  |
| [15,37,57] | Glass fibre/epoxy | Cohesive element    | $10^8/10^8$                         | 39.1/39.1                         | 100/100  |
| [54]       | Glass fibre/MTM57 | Cohesive element    | 100/100                             | –/100                             | –/100  |
| [55]       | HTA/6376          | Cohesive element    | $10^5/10^5$                         | 15/15                             | 2.5/2.5  |
| [4,21,60]  | AS4/8552          | Cohesive surface    | $10^8/10^8$                         | 57/85                             | 7/80   |
| [44,62]    | HTA/6376          | Cohesive element    | $10^8/10^8$                         | 70/80                             | 2/32   |
| [58,64,65] | TC33/epoxy        | Cohesive element    | $8.46 \times 10^5/5.35 \times 10^5$ | 27.5/45                           | 5/100  |

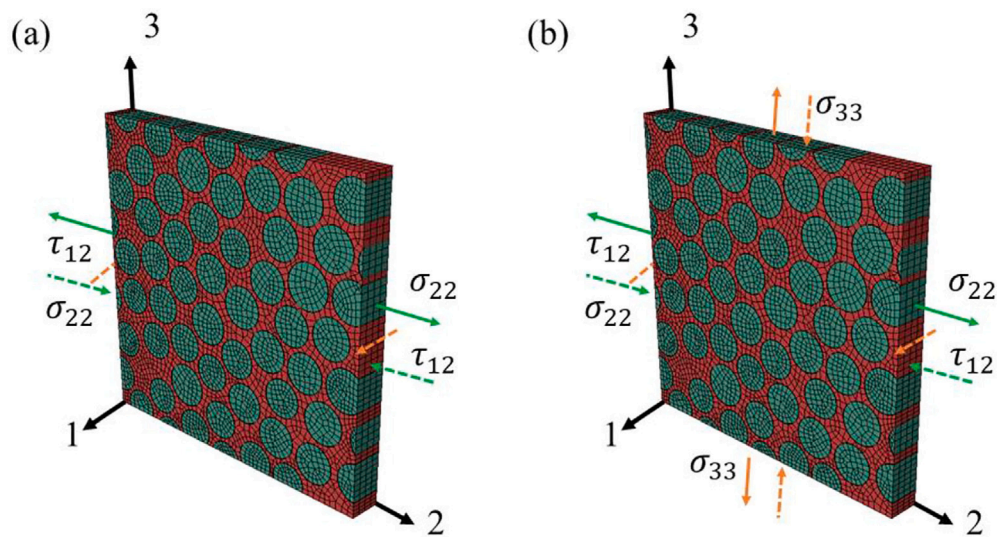


**Fig. 4.** RVE subjected to different loads: (a) combined transverse tension/compression and in-plane shear loadings; (b) transverse, out-of-plane tension/compression and in-plane shear [50].

and diagonal arrangements of fibres were considered in the unit cell modelling within the framework of FEM. Von Mises yielding criterion and dilatational energy density criterion were adopted to determine the yielding and brittle fracture zones, respectively. Not accounting for fibre–matrix interface debonding, they found that the cavitation-induced brittle failure occurred earlier than the matrix yielding. Fibre modules were found to have a significant effect on the composite failure caused by cavitation in the matrix. Cavitation occurs when the hydrodynamic pressure exceeds the vapour pressure of a moving liquid [69]. During the manufacturing process of composites, the cavitation stays inside the matrix in the form of voids. Ha and co-workers [70–72] conducted extensive analysis on the effects of fibre arrangement and interface properties on the failure prediction of composites based on unit cell modelling under different loading conditions. The mechanical performance of CFRP composite materials was conducted on a unit cell and a random model by Trias et al. [73,74]. The simulation results suggested that the periodic unit model can be used for the prediction of effective properties, but leads to underestimation of matrix cracking and damage initiation. This is mainly due to the fact that damage initiation always starts in the highly strained locations in the matrix and fibre/matrix interface, which is hard to be captured by the periodic unit model. Thus, the random model should be used for failure and damage simulations. They also pointed out that the minimal size of an RVE is

$\delta = \frac{L}{R} = 50$ , where the  $L$  and  $R$  are the side length of the RVE and the fibre radius, respectively.

With the aforementioned approaches of synthetically generating the random fibre distributions, Vaughan and McCarthy [55] examined the influence of fibre/matrix debonding on the failure prediction of a CFRP composite under transverse tension. They found that the mechanical properties of the fibre–matrix interface greatly influenced the failure behaviour of the material, in which the interfacial strength controls the overall transverse strength, while the interfacial fracture toughness increased ductility to resist fracture. A similar failure analysis was conducted by Moraleta et al. [75], which found that the onset of damage and tensile strength was controlled by interface strength while the evolution of damage depended on interface toughness. Shang and Shi [76] analysed the effect of Weibull distribution-based stochastic fibre/matrix interface strength on the tensile behaviour of fibre-reinforced composites (FRC) and they concluded that Weibull shape parameters can result in different transverse tensile strength and failure path. Yang et al. [37] have studied the mechanical behaviour of UD FRP composites subjected to transverse tension and compression using computational micromechanics. An RVE with a random fibre distribution was used, and matrix plastic deformation and interface debonding were included with the help of the extended Drucker–Prager model and cohesive element, respectively. A ductile damage initiation criterion and a damage evolution model were introduced to simulate the damage of the matrix. The

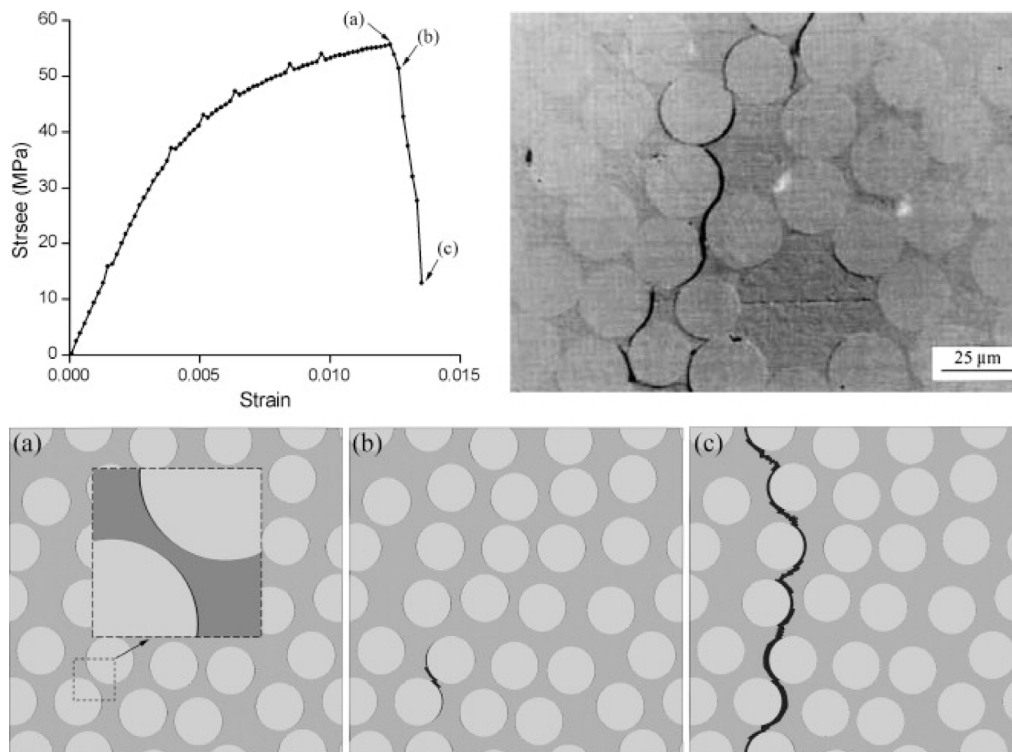


Fig. 5. Numerical simulation of damage initiation and evolution under transverse tension [37] and the experimental result [77]. (Points a, b and c on the stress–strain curve represent three different stages in the progressive damage process, which are corresponding to the different damage states, respectively. A crack plane, perpendicular to the loading direction, which connects matrix and fibre/matrix interface cracks, was predicted in excellent agreement with experimental findings.).

progressive failure analysis of composites suggested that the tension-induced damage starts from the interface debonding and propagates as a result of interactions between interface debonding and matrix plastic deformation, see Fig. 5; while the compression failure is dominated by matrix plastic damage, with a shear band inclined at  $52.5^\circ$  with respect to the plane perpendicular to the loading axis, see Fig. 6. González and Llorca [15] conducted the progressive failure analysis of carbon fibre/epoxy composites with a micromechanics-based RVE using periodic boundary conditions. The M–C constitutive model and cohesive zone model at the fibre/matrix interface were used to describe the behaviour of the constituent phases. They found that the mechanical properties of composites under transverse compression were mainly controlled by interface strength and matrix yield strength. Two dominant damage mechanisms were identified, depending on whether the failure was controlled by the nucleation of interface cracks or by the formation of matrix shear bands.

Yang et al. [57] performed micromechanical failure analysis of unidirectional composites on an RVE with randomly distributed fibres using periodic boundary conditions. The simulation results of the unidirectional composites under shear loadings indicated that failure of the composite lamina subjected to in-plane shear is initiated by interface debonding and the ultimate failure is due to the matrix damage, while the damage under transverse shear is dominated by the matrix plastic damage. Totry et al. [54] studied the effects of the mechanical properties of fibre, matrix and interface on the mechanical performance of CFRP composites under in-plane and out-of-plane shear using experiments and numerical simulations, see Fig. 7. It was found that the in-plane shear behaviour of composites was controlled by the matrix yield strength and the interface strength and was independent of the fibre properties. O'Dwyer et al. [78] quantified the shear hardening effect in the failure analysis of composites with a micromechanics-based RVE model under in-plane shear. It was found the observed global strain hardening effect came from the rotation of fibres. Vaughan and McCarthy [79] presented a high-fidelity RVE model to examine the

influence of interface properties on the mechanical performance of a CFRP composite under transverse shear. The fibre–matrix interface strength was found to control transverse shear strength, while the interface fracture energy had a marked effect on the strain to failure and the interaction of damage mechanisms during fracture. Melro et al. [33,43] developed a constitutive model for an epoxy matrix with a thermodynamically consistent elasto-plastic with a damage material law. The influence of different yielding strengths under tension or compression and hydrostatic pressure was considered; also, an isotropic damage model was included. Regularisation of dissipated energy was implemented by using the characteristic length of elements and fracture toughness to guarantee mesh size independence and the consistent tangent operator was determined to ensure convergence. Afterwards, they implemented this damage model for the epoxy matrix into the FE RVE modelling of the unidirectional composite, in which different loading conditions were considered for the prediction of the damage initiation and propagation in the matrix and interface. They found that interfacial damage is responsible for the damage initiation in composites when subjected to transverse tension and transverse shear loadings, while the matrix is solely responsible for damage initiation and propagation under longitudinal shear load.

Modelling fibre-dominated failure of UD composites is another challenge due to the complex interplay of damage mechanisms under longitudinal loadings. Several important aspects should be covered in the high-fidelity RVE modelling under longitudinal loadings, such as the stochastic fibre tensile strength along the length, the kinking band under longitudinal compression as well as the debonded length of a broken fibre. Blassiau et al. [80–82] investigated the effects of the viscoelastic matrix and fibre/matrix interface debonding on the load transfer from the broken fibres to neighbouring intact fibres by shear of the matrix based on unit cell modelling, with the consideration of the stochastic nature of fibre strength along the fibre length. Wang et al. [83] used bilinear cohesive elements to represent the matrix/fibre interface in a single fibre unit cell model, in which the failure is

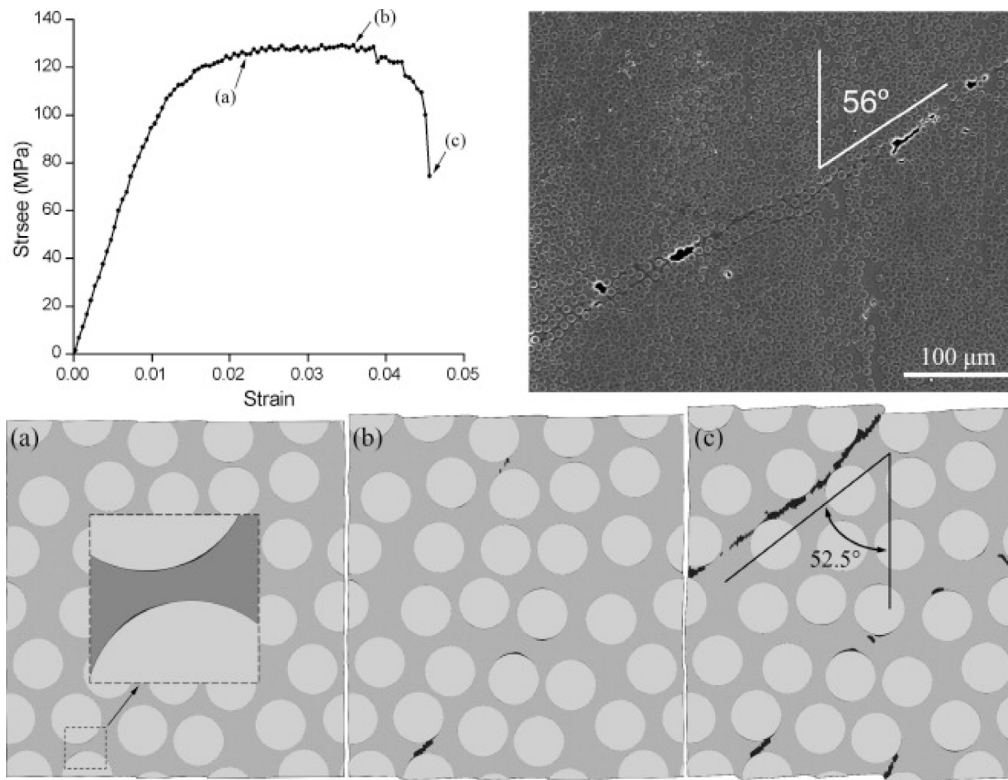


Fig. 6. Numerical simulation of damage initiation and propagation under transverse compression [37] and the experimental result [15]. (Points a, b and c on the stress-strain curve represent three different stages in the progressive damage process, which are corresponding to the different damage states, respectively. A shear band of around 52.5° was predicted with respect to the plane perpendicular to the loading direction, compared to the 56° observed experimentally.).

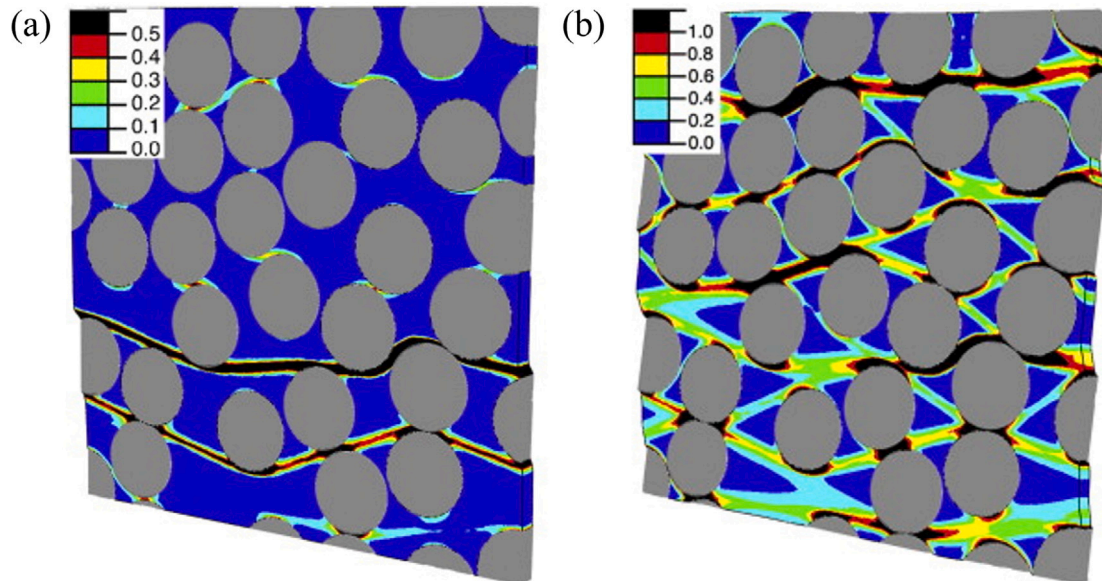


Fig. 7. Contour plot of the accumulated plastic shear strain in the matrix: (a) at the in-plane shear strain of 6.0% and (b) at the out-of-plane shear strain of 20% [54]. (Two main shear bands were predicted in the in-plane shear loadings while multiple random shear/crack planes were predicted in the out-of-plane shear loadings due to the interaction of fibre/matrix interface cracks and matrix cracks.).

determined by the energy-based damage evolution law. It was observed that the damage in composites initiates by fibre breakage, which causes the interface failure, followed by matrix cracking. In addition, the simulation results suggested that the interface strength begins to influence the deformation behaviour of the composite material only after the fibre is broken. Mishnaevsky and Brøndsted [84,85] conducted deformation and damage analysis for unidirectional fibre-reinforced

composites subjected to longitudinal tension with 3D RVE models. In their analysis, the numerical finite element weakening was introduced for the modelling of fibre cracking and interface damage. In order to take random fibre fragments into consideration, potential fracture planes were randomly arranged along the fibre length, the location of which was determined by a normal distribution. They modelled the fibre/matrix interface as a homogeneous and isotropic third layer with a

certain thickness. The influences of matrix cracks and interface strength on fibre failure were numerically investigated. However, the interface was modelled as a rather brittle layer, which is not always true in realistic case. Naya [86] conducted failure analysis of CFRP composites under longitudinal tension using 3D high-fidelity RVE models, in which the composite microstructure is idealised as a dispersion of parallel and circular elastic fibres embedded in the polymer matrix. The fracture of fibre is represented by a set of fracture planes [45,87], modelled by cohesive surface-based interaction in a certain region of every fibre. The effects of fibre distribution, constituent properties and residual thermal stresses were discussed. The effect of fibre misalignment on the failure strength of CFRP composites was studied by Luis et al. [20].

Failure prediction and kinking band formation of FRP composites under longitudinal compression has been widely investigated in the last few decades. Numerical micromechanics-based modelling offers important insights into understanding fibre kinking mechanisms. Kyriakides et al. [88] constructed a 2D FE model of a layered composite made of fibre and elasto-plastic matrix, in which the initial fibre misalignment is represented by a sinusoidal curve. The kinking band formation was successfully captured by the model. Hsu et al. [89,90] developed 3D micromechanics FE models to assess the limitations of 2D models on the failure prediction of composites under longitudinal compression. They found both models were in good agreement for the compressive failure strength, while the plasticity parameters should be calibrated separately. The width and inclination of the kink band were found to be larger than the 3D models in the post-peak predictions. Thus, a follow-up study on the post-peak behaviour of composites was conducted with an improved 3D model. Fibre kinking initiation and kinking band broadening or propagation was systematically investigated experimentally and numerically by Vogler et al. [91,92]. They observed that the onset of failure is a dynamic event, resulting in kinking of fibres. The kinking band propagation is driven by shearing, in which the propagation stress is rate sensitive. Such a phenomenon was successfully reproduced by the numerical models, in which the material is idealised as a hexagonal array of round elastic fibres in an elastic-power law visco-plastic matrix. The interaction between fibre kinking and fibre splitting was investigated by Prabhakar et al. [93] with a 2D finite element model. A typical instability behaviour with a sharp peak and a snap-back branch was found in the numerical simulation with a perfect fibre/matrix interface, thus a discrete cohesive zone model was applied at the interface. They also pointed out the importance of the shear strength of the interface in the determination of compressive strength and failure mode of composites under longitudinal compression. More recently, 3D high-fidelity RVE models were developed to investigate the effects of mechanical properties of constituents, friction between fibre and matrix, initial fibre waviness angle and misalignment and environmental conditions on the failure strength of CFRP composites in [17,21,44,59,94].

Although some failure problems of composites are still under investigation, i.e. fibre kinking under longitudinal compression. These high-fidelity models are proved to be an effective approach to replace time-consuming and expensive physical experiments, if not, at least for material screening purposes. These models can provide full control of the microstructure, constituents properties, and loading conditions, such as complex multiaxial stress states which cannot be applied experimentally. This allows the microstructure optimisation and tailoring as well as failure criteria assessment to be possible, which is discussed in the next section.

### 3. Microscale modelling of composites with DEMs

FEM becomes dominant in the analysis of the progressive failure of FRP composite due to their solid physical foundation and rigorous mathematic formulations. However, since it is based on the continuum mechanics, the stress/strain conception may not be applied when discontinuities emerge. Even though the discontinuity problems can be

addressed by redefining a body to exclude the crack and applying new boundary conditions to the crack surfaces, a mesh refining technique is still needed. Moreover, FEM still suffers from the requirement of an additional damage criterion to guide the damage propagation, and capturing the multiple damage modes interaction remains challenging for FEM. Recently, the discrete element method (DEM) emerges as a promising approach in the progressive failure analysis of composite materials, due to some of its inherent advantages over the FEM, such as its capability of dealing with damage initiation in unguided locations, damage propagation along unguided paths and complex multiple damage modes interaction in FRP composites. Here in this section, the DEM theory and the application of DEM in the progressive failure analysis of FRP composites are reviewed and discussed.

#### 3.1. 3D DEM theory

DEM was firstly proposed by Cundall [95] and extended by Cundall and Strack [96] within the context of rock mechanics. In the DEM, the interaction between contacting particles is treated as a dynamic process and the stress and deformation of the whole particle assembly are obtained from the average of the force and displacement of each individual particle. The contact which connects the two particles can be physically represented via springs, friction resistance and damp absorber, as shown in Fig. 8 [97].

The dynamic behaviours of particles in DEM are completed through the integration of particles' accelerations and velocities by using a central-difference scheme with an explicit time-step algorithm [14]. The calculation of DEM is alternatively performed by Newton's second law and force-displacement law. Newton's second law is used to calculate the particle's acceleration resulting from the contact forces and external forces, while the force-displacement law is used to update the contact forces according to the relative displacement of the two contacting particles. These two laws are repeatedly applied during the whole calculation cycle of the DEM simulation for one timestep. Thus, DEM is suitable to dynamically simulate the particle systems, in which the movement of every particle is essential to monitor and analyse. The discrete particles can also be densely packed and bonded together by adding special bonds at the contact points corresponding to special constitutive equations.

#### 3.2. Bonded particle model in 3D DEM

Particles in DEM can be bonded together at contacts and separated when the bond strength or energy is exceeded, thus the behaviour of bulk materials can be simulated by assembling particles through bonds at contacts. The advantage of this method is that the two bonded particles can be separated and thus a crack is formed at the contact point once the failure condition of the bond is satisfied. In a DEM model, elementary micro-scale particles are assembled to form the bulk material with macroscopic continuum behaviour determined only by the dynamic interaction of all particles. Unlike the conventional FEM which is based on the traditional continuum mechanics and provides stress and displacement solutions by solving a global stiffness matrix equation, DEM is discontinuous and the information of each particle element and contact is recorded individually and updated dynamically. Thus, DEM is convenient to deal with the local behaviour of the material by defining local models or parameters for the specified particles and contacts. Subject to external loading, when the strength or the fracture energy of a bond between particles is exceeded, flow and disaggregation of the particle assembly occur and the bond starts breaking [14]. Consequently, cracks form naturally at the micro scale. Hence, damages and their interaction emanate as the process of debonding of particles. The way that DEM discretises the material domain gives the most significant advantage over the traditional continuum methodologies, such that problems like the dynamic material behaviour of composites, crack tip singularities, and crack formulation criteria can

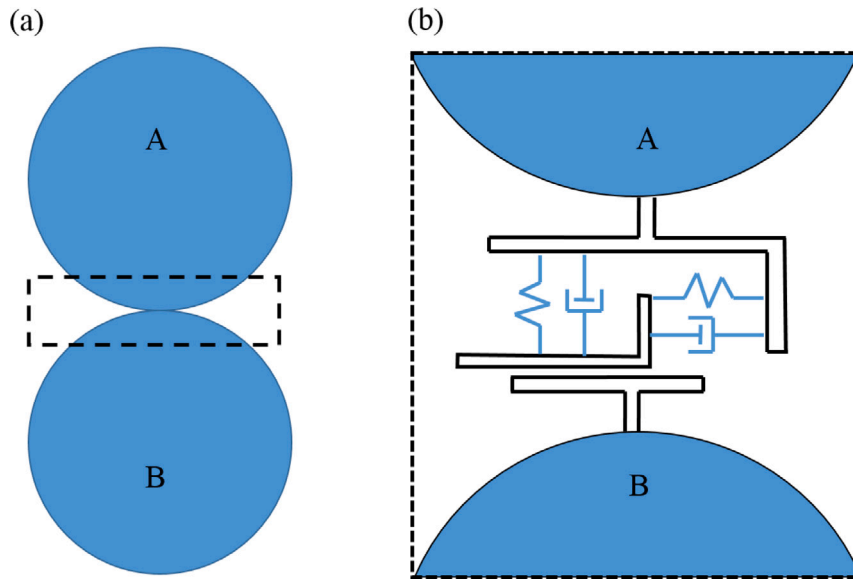


Fig. 8. A contact between two particles in a 3D DEM model: (a) two particles in contact and (b) the physical elements of the contact [97].

all be avoided due to the naturally discontinuous representation for material microstructure via particle assemblies. Therefore, DEM has been applied in the simulation of crack or damage in rock [98], concrete [99], ceramic [100] and composite materials [101].

Bonds in DEM can be envisioned as a kind of glue joining the two contacting particles. For example, a parallel bond can be regarded as a set of elastic springs with constant normal and shear stiffness, uniformly distributed over either a circular or rectangular cross-section lying on the contact plane and centred at the contact point, as shown in Fig. 9 [14]. Fig. 9(b) and (c) represent the behaviour and components of the linear parallel bond model in normal and shear directions, respectively.  $\bar{k}_n$  and  $k_n$  are the normal stiffness of the parallel bond and particles, respectively.  $g_s$  and  $\bar{\sigma}_c$  are the surface gap and tensile strength of the parallel bond, respectively.  $\bar{k}_s$  and  $k_s$  are the shear stiffness of the parallel bond and particles, respectively.  $\mu$  is the friction coefficient in the linear model and the  $\bar{c}$  and  $\bar{\phi}$  are the cohesion and friction angle in the parallel bond model, respectively. A parallel bond can transmit both force and moment.

In the DEM model with parallel bonds, the contact stiffness,  $K_i$ , at each particle–particle contact is resulted from both particles' stiffness and parallel bond's stiffness through the following formulations [14],

$$K_i = A\bar{k}_i + k_i \quad (19)$$

$$A = 2\bar{R}\delta \quad (20)$$

$$K_i = \frac{k_i^{[A]}k_i^{[B]}}{k_i^{[A]} + k_i^{[B]}} \quad (21)$$

where  $\bar{R}$  and  $A$  are the radius and cross-section area of the parallel bond, respectively.  $\delta$  is the element thickness,  $\bar{k}_i$  is the parallel bond stiffness and  $k_i$  is the equivalent stiffness of the two contacting particles.  $i$  is in place of  $n$  or  $s$ , which indicates normal or shear direction, respectively.

The constitutive law of the parallel bond is defined by a relationship between the traction and the relative displacement at the interface, see Fig. 10. The failure criterion of the interface bonds is based on the Energy Release Rate concept. Since the bond-based DEM model implies the absence of stress singularities at the crack tip, the ERR in an interface model can be defined as the elastic strain energy per unit length stored in the unbroken bonds at the crack tip [104,105]. In the constitutive model (Fig. 10(a)), the normal stress increases with the elongation of the bond between two adjacent particles and reduces to zero when it exceeds the corresponding strength  $\bar{\sigma}_{nc}$ . It should be noted

that normal the strength  $\bar{\sigma}_{nc}$  is calculated from the critical fracture energy  $G_{IC}$ , i.e. the grey triangle area in Fig. 10(a). The normal stress is calculated from  $\bar{\sigma}_n = \frac{\bar{F}_n}{A}$ . For the broken bond in the normal direction in Fig. 10(b), it is deleted when the normal stress exceeds the strength and no longer holds stress between two particles. The shear strength  $\bar{\sigma}_{sc}$  and stress  $\bar{\sigma}_s$  of the bonds are calculated from critical fracture energy  $G_{IIC}$  and force  $\bar{F}_s$  in the tangential direction, respectively. The constitutive model of the bonds in the tangential direction for the undamaged and damaged interface can be seen in Fig. 10(c) and (d), respectively.

When a bonded particle model is used in DEM to represent solid materials, one first needs to determine the bond and particle stiffness in the model ('micro-stiffness') so as to represent the elasticity ('macro-stiffness') of the real target material. In principle, it is possible to establish a theoretical relationship between the micro and macro stiffness when particles are packed in a regular form and a unit cell can be identified. The formulation for square or hexagonal bonded particles in 2D DEM models of both isotropic and orthotropic materials have been reported in previous literature either using average strain energy method [106,107] or discrete element method [108,109]. The regular packing of 3D particles is much more complex, even just for a DEM model of isotropic material. Zhao et al. [110] applied the internal bond method and average strain energy method to correlate the bond stiffness with the real material elastic stiffness.

### 3.3. Failure prediction of composites under uniaxial loadings

A 3D RVE based on DEM modelling was conducted by Maheo et al. [111] to study the local mechanism of failure degradation of a UD CFRP composite subjected to different loading conditions, including matrix micro-cracking, interface debonding and fibre breaks. A simple brittle elastic behaviour is adopted for fibre and matrix to prove the feasibility of this method. Two failure criteria, "breakable bonds failure criterion" and removed discrete element failure criterion", were implemented into the DEM model for an assessment of the capabilities of the DEM for modelling the damage of the composite materials.

A novel approach was proposed by Ismail et al. [112] to generate the random distributions of fibres in the RVE of CFRP based on the DEM and validated with the results of FEM as well as the experimental findings. This approach was applied to investigate the progressive failure of FRP composites under transverse tension [113], transverse compression [114], out-of-plane shear [114] and combined transverse compression and out-of-plane shear [114]. The simulation

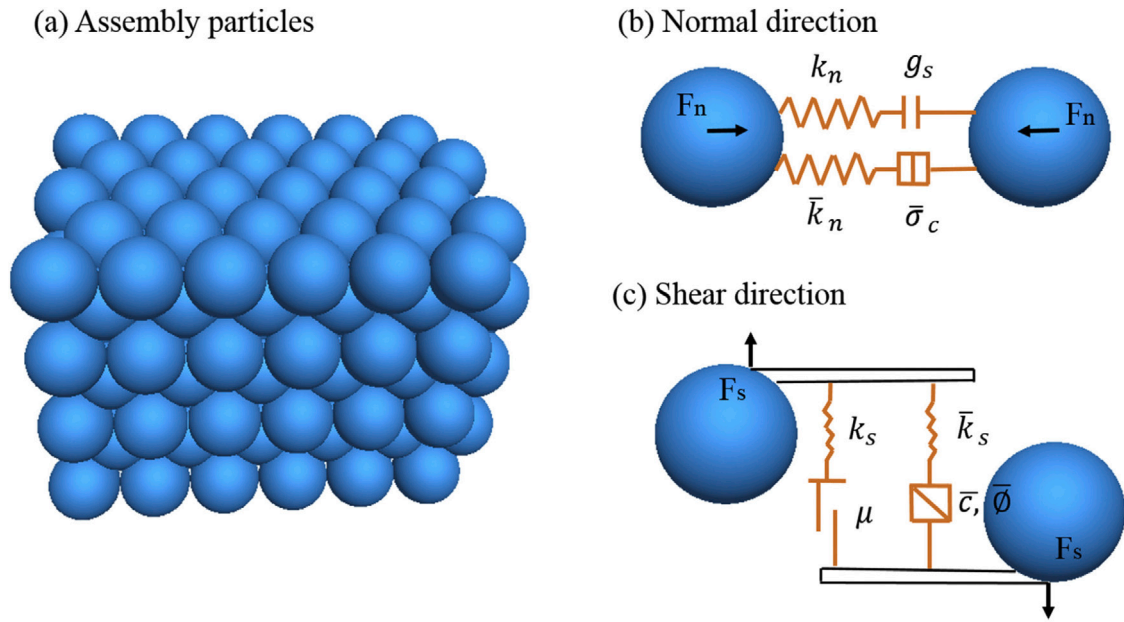


Fig. 9. Parallel bond illustration in DEM: (a) a representative model of assembly particles using DEM, and the schematic of the parallel bond with physical parameters in (b) normal direction and (c) shear direction [97].

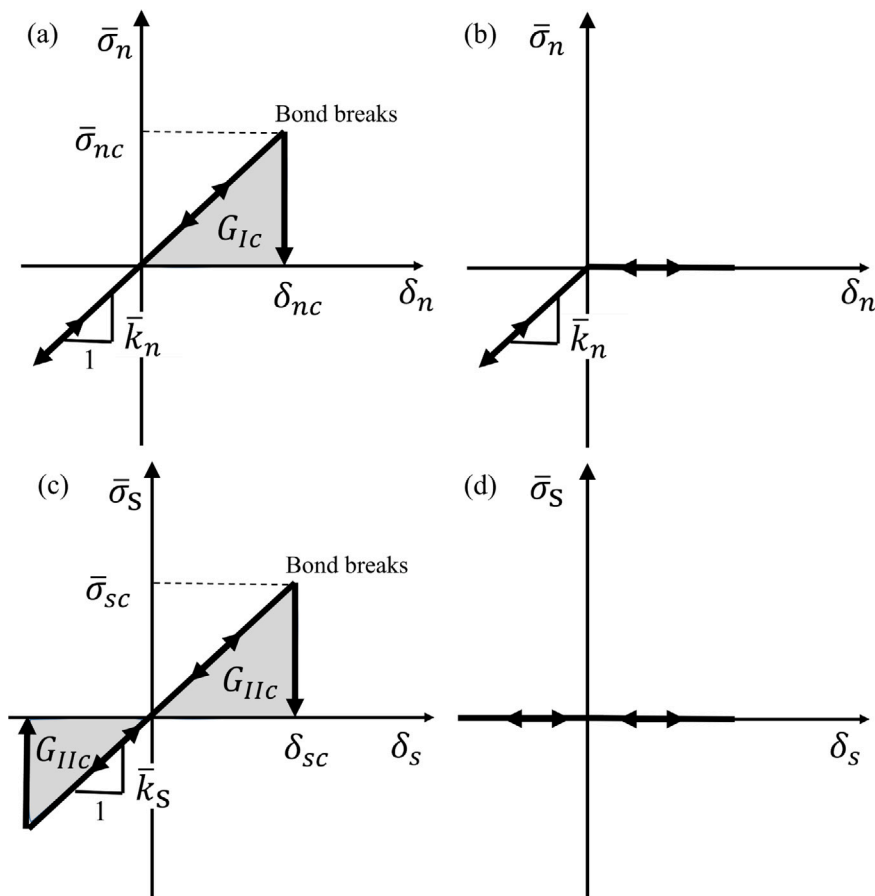


Fig. 10. Linear elastic brittle law of the parallel bond in the normal direction for (a) an undamaged interface and (b) a broken interface, and in the tangential direction for (c) an undamaged interface and (d) a broken interface [102,103].

results showed that the DEM model is able to predict the damage initiation and propagation of composites under the aforementioned loading conditions, see Fig. 11 for the progressive failure process under transverse tension.

Sheng et al. [115] investigated the effect of fibre distributions on the transverse cracking based on DEM modelling, such as rectangular, hexagonal and random fibre distributions. The unguided damage onset and progression of matrix cracking as well as interfacial

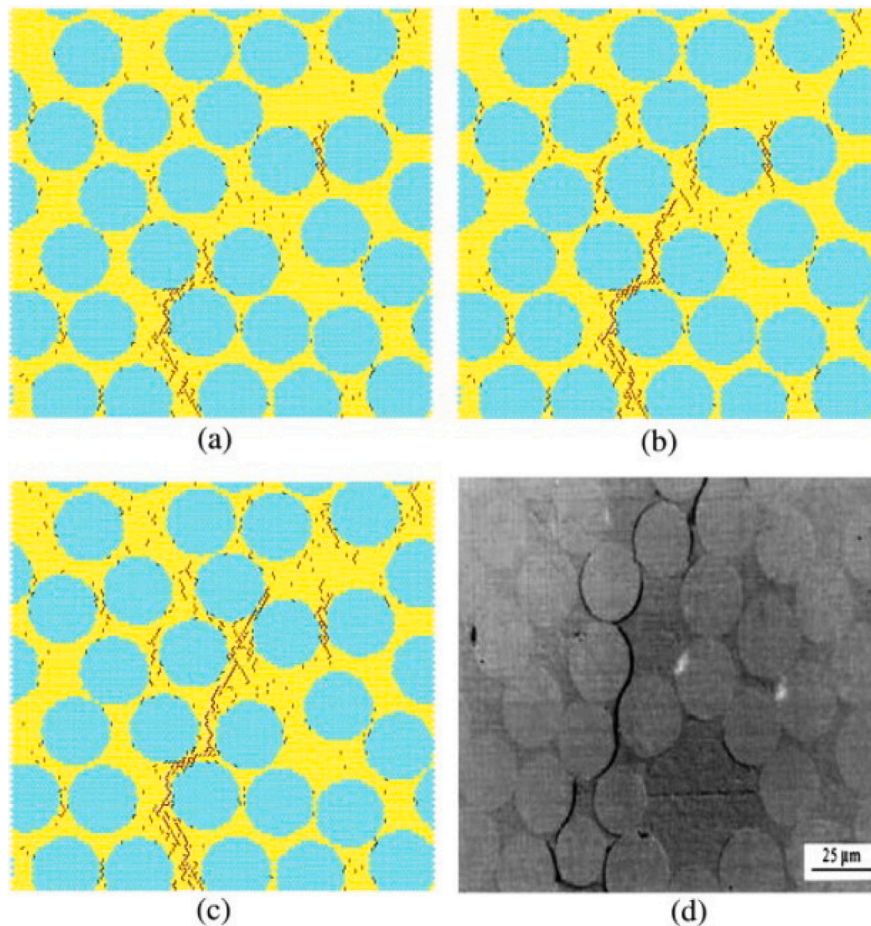


Fig. 11. Damage initiation and progression under transverse tension at different strain [113]: (a) Strain of 0.007, (b) Strain of 0.01, (c) Strain of 0.014 and (d) Experimental results [15] (red lines represent the matrix cracks and black lines represent interface debonding). (For interpretation of the references to colour in this figure legend, the reader is referred to the web version of this article.)

debonding were well captured. It was found the damage propagation path and material behaviours of matrix and fibre/matrix interface are both influenced by the spatial distributions and volume fraction of fibres.

Ding et al. [116] developed two back-propagation deep neural networks (DNNs) based models to investigate the mechanical properties and microscopic crack patterns of FRP composite laminae. 2000 RVE models based on DEM with 200 different sets of fibre volume fractions and fibre radii were used to generate a database to train the DNN-based regression model. 1600 DEM simulations with a fixed 45% fibre volume fraction and  $3.3 \mu\text{m}$  fibre radius were conducted to train the DNN-based classification model. Good accuracy was achieved regarding the prediction of mechanical properties and crack patterns.

#### 4. Failure prediction of composites under multiaxial loadings and failure criteria assessment

Essentially, the failure of composite materials is a very complicated process due to the inherent nature, such as the microstructure, material properties, complex loadings and manufacturing defects [117]. Thus, the failure criteria, in order to determine the design space, are vital in the design and failure analysis of composite structures under complex loading conditions [44]. Over several decades, numerous failure criteria were proposed, including but not limited to strain-based [118], strain–energy-based [119], stress-based [120–123] and phenomenological failure criteria [124–129]. An essential part of advancing state-of-the-art damage models and criteria is to validate their predictions with the experimental findings. However, model/criteria

validation remains challenging due to the lack of enough experimental data, especially under multiaxial loadings. For example, Gutkin et al. [130] pointed out that the experimental determination of the failure envelope for a case of combined longitudinal compression and in-plane shear is a complex, time-consuming and material-consuming process. Even though different types of set-ups (e.g. cruciform test set-up or torsion/compression of tubes) can be accessible to obtain the required failure point, the required stress state is still challenging due to free edge effects or changes in geometry. In addition, the longitudinal compression failure strength is particularly sensitive to material defects and imperfections of the testing set-up, resulting in multiple repeatable tests. An objective assessment of widely used failure criteria for fibre-reinforced composites was conducted under different loadings in a series of three World Wide Failure Exercises [131–138]. It was found that nearly all of the theories could give accurate predictions of strength and strain in the targeted laminates at small strains before initial failure, but few of them could deal with the failure problem under multiaxial loadings. Meanwhile, the influences of ply thickness, lay-up sequence, size effects on failure strength as well as the interaction between cracks in differently oriented adjacent layers and delamination driven by matrix cracking were investigated. However, a consensus was not reached on the abovementioned studies. Thus, precise conclusions were not reached regarding which criterion can best reproduce the physical failure mechanisms and the mechanical strength because of the scarcity of the experimental data, especially under multiaxial stress states, resulting in many failure criteria not being fully validated.

With the rapid development of computing power, the aforementioned limitations from analytical and experimental approaches have

been addressed by computational micromechanics analysis. With the development of 3D high-fidelity RVE models, more studies are capable of dealing with the progressive failure analysis and criteria assessment of UD composites subjected to biaxial loadings, such as transverse tension and out-of-plane shear [44,139], transverse compression and out-of-plane shear [44,56], transverse compression and in-plane shear [4,44,46,58], transverse tension and in-plane shear [4,44,58], longitudinal tension and transverse compression [45] and longitudinal compression and in-plane shear [130] and triaxial stress states [50].

Llorca and co-workers [56,139] investigated the progressive failure behaviour of UD composites subjected to combined transverse tension/compression and in-plane shear and assessed Hashin, Puck and LaRC failure criteria. A strong and a weak interfaces were introduced by inserting cohesive elements between fibres and matrix to predict the failure strengths of composites, which were used to assess the failure criteria. It was found that the failure criteria agreed with the failure strengths predicted by numerical simulations of the composites with a strong interface but overestimated the composite strength with a weak interface as interface decohesion was not taken into account. These results suggest the need for interface fracture into the failure criteria for composite failure prediction. Failure analysis of CFRP composites was conducted and more failure criteria were assessed under combined transverse and in-plane shear in [4,44,54,58] using 3D high-fidelity RVE models. It was found that Hashin failure criteria agree well with the numerical results with a weak interface, while Puck, LaRC05 failure criteria agree well with the numerical results with a strong interface. The reason why Hashin failure criteria underestimate the failure strength under combined transverse compression and in-plane shear may be due to the negligence of shear hardening under transverse compression [21]. Different failure modes were predicted and progressive failure mechanisms were discussed with a strong and a weak interfaces are taken into account [56,58] under transverse and in-plane shear. The transition points for different failure modes were also determined based on the failure analysis of CFRP composites. Sun et al. [44] conducted a failure analysis of CFRP composites under transverse and out-of-plane shear, it was found that the damage is always initiated by the nucleation of interface cracks and propagates along the weakest path, and fails when the coalesce of interface cracks through the matrix is formed. The comparison of failure envelopes predicted by classical failure criteria and numerical simulations can be found in Fig. 12. It was found that all failure criteria fail to give satisfactory results for combined loadings.

A micromechanics-based hexagonal unit cell was developed to predict the failure strength of an FRP composite lamina subjected to transverse compression and longitudinal tension [45]. Nonlinear cohesive elements were inserted into the damageable section of fibres and placed between the fibre and matrix, while the nonlinear plasticity of the matrix was modelled by the D–P plastic criterion. Fibre failure mode and matrix failure mode were captured by the unit cell under the biaxial loadings. It was found that the failure strength obtained from numerical simulations agreed better with the experimental results than those predicted by Puck failure criteria. A 2D micromechanics-based model was developed to investigate the failure mechanisms and assess failure criteria of CFRP composites under longitudinal compression and in-plane shear [130]. The effects of fibre, matrix properties and misalignment on failure strength were studied. It was found that the failure envelope is defined by two regions corresponding to different failure mechanisms: shear-driven fibre compressive failure and fibre kinking/splitting. It was found that both Jelf and Fleck kinking model [140] and LaRC05 kinking criterion [141] can capture the linear trend in the region on the failure envelope where matrix failure is the dominated failure mode when the shear behaviour of the composite is linear. However, only the LaRC05 kinking criterion [141] can capture the concave-shaped trend when the nonlinearity of the composite material is accounted for. Sun et al. [44] constructed 3D high-fidelity

micromechanics-based RVE models to predict the failure strength of UD composites under different combined biaxial loadings and assessed widely used failure criteria. Three phases were considered in their RVE modelling, including fibre, matrix, an interface represented by cohesive elements between the fibre and interphase, and an interphase region represented by the same model as the matrix between interface and matrix. The effects of fibre waviness angle on the failure envelope were conducted and failure modes were captured by the RVE model, see Fig. 13. New homogenised failure criteria based on NU-Daniel failure criteria [142,143] were proposed, considering transitions of failure mechanisms, for UD CFRP composites. It was found that the numerical results obtained from the newly proposed failure criterion agree with the experimental findings.

Ye et al. [144] investigated the failure of FRP composites subjected uniaxial and biaxial loadings coupled with temperature variations based on High Fidelity Generalized Method of Cells (HFGMC) [145, 146]. Tsai–Hill failure criterion was applied for the stiffness degradation and failure prediction of a unit cell of composites under thermo-mechanical loadings. It was found that the temperature has insignificant influences on the final failure of composites, and the maximum stresses in the composites are always located in the vicinity of the interface under uniaxial and biaxial loadings. Biaxial failure envelopes of the off-axis composites under thermo-mechanical loadings were plotted. More recently, they applied four-fibre RVE models based on parametric finite-volume direct averaging micromechanics (FVDAM) [147] to study microscale damage propagation of composites with initial voids/defects under uniaxial and biaxial loadings [148]. Hashin failure criteria were applied to predict sub-cell failure. Three different types of initial defects were introduced and the effects of these defects (i.e. location, distribution and orientation) on damage propagations were studied.

Chen et al. [50] conducted a preliminary study on the failure prediction of unidirectional CFRP composites under triaxial loadings with micromechanics-based RVE modelling and artificial neural networks. A hybrid loading strategy was proposed to apply triaxial loading. Failure points on sliced surfaces in the triaxial stress space were obtained with constant stress in the third direction. It was found that with only 560 samples, an ANN model with two hidden layers can achieve 97.5% accuracy for the classification problem of failure. Interestingly, the predicted 3D failure surface has an elliptical paraboloid shape and shows an extremely high strength in biaxial compression, which is worthy of further investigation.

## 5. Concluding remarks

Considerable efforts have been made for the development of suitable numerical models to reliably predict the progressive failure process of fibre-reinforced composite materials. This paper presents a comprehensive review of research works on modelling strategies of representative volume elements, including the generation of spatial fibre distributions, constitutive modelling and periodic boundary conditions, and progressive failure analysis of FRP composites under various loading conditions as well as the failure criteria assessment under multiaxial stress states. The main conclusions and some noteworthy issues are summarised as below:

- The random fibre distribution close to reality is necessary to conduct micromechanical failure analysis of composites. Three approaches, namely experimental, coupled experimental–numerical and numerical ones, have their own strengths and drawbacks. A balance between the accuracy of numerical simulations and numerical convergence needs to be considered when selecting a suitable model to generate random fibre distributions.

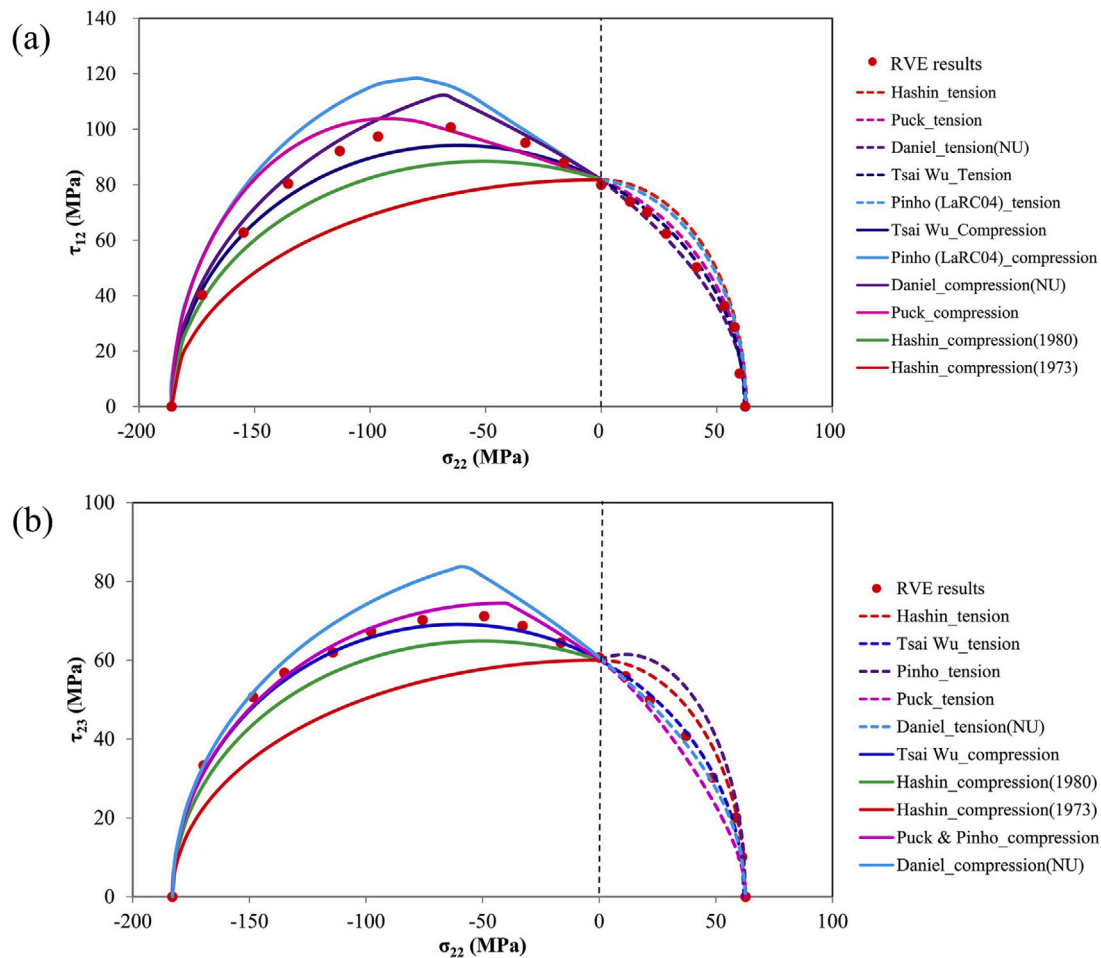


**Fig. 12.** Comparison of failure prediction between classical failure criteria and numerical simulations under (a) transverse compression and in-plane shear, (b) transverse compression and out-of-plane shear [44]. (Solid lines represent the failure envelopes predicted by different failure criteria under combined transverse compression and in-plane/out-of-plane shear, and dash lines represent the failure envelopes predicted by different failure criteria under combined transverse tension and in-plane/out-of-plane shear. Different colours represent different failure criteria. Red dots represent failure points predicted from numerical simulations under biaxial loadings. No failure criterion was found to accurately predict the failure strength under both biaxial loadings). (For interpretation of the references to colour in this figure legend, the reader is referred to the web version of this article.)

- Fibre models: linear elastic and/or brittle models are used to capture the mechanical response of fibres depending on loading conditions; Matrix models: Mohr–Coulomb plastic, Drucker–Prager plastic model and Ductile damage initiation law, Drucker–Prager plastic damage model and Melro’s model [33] are briefly discussed and compared under uniaxial and multiaxial loading conditions; Interface models: the cohesive zone models are briefly recovered and the improvement of the models are discussed.
- The mechanical properties and progressive failure process of FRP composites can be predicted with a great accuracy against experimental findings. Damage is initiated by interface debonding and/or matrix cracking in the matrix-dominated failure cases, while fibre breakage occurs first in the longitudinal tension case. The failure mechanisms of FRP composites considering fibre kinking are still under investigation, although some key features of fibre kinking can be captured by 3D high-fidelity RVE models.
- Conventional failure criteria under various multiaxial stress states can be assessed and compared using computational micromechanics-based RVE models. It was found that the fibre/matrix interface plays a vital role in determining the failure strength of composites under multiaxial stresses, thus suggesting a necessity of including interface into the construction of failure criteria within the framework of multiscale analysis.
- FEM offers a great potential in the progressive failure analysis of FRP composites and becomes dominant in industry and academia

due to its solid physical foundation based on continuum mechanics that permit a rigorous description of mechanics. However, it is still challenging to deal with discontinuity issues, especially considering damage propagation, which leads to more advanced FEM algorithms, such as the extended FEM (X-FEM) and the augmented FEM (A-FEM).

- DEM can be an efficient approach to generating random fibre distributions, with high volume fractions and specified inter-fibre distances, for microscale failure analysis of UD FRP composites. With simple linear elastic brittle parallel bonds, the elastic mechanical properties of a DEM model of composites with bonded particles can be accurately predicted based on the average strain energy method when the particles are packed regularly. Failure analysis can be conducted with failure criteria applied to the parallel bonds.
- Multiaxial failure analysis of UD FRP composites was conducted using DEM, in which the matrix was modelled with parallel bonds while the fibre/matrix interface was modelled with a softening bond. The strength of the bonds used in the DEM model was calibrated from experiments.
- DEM can be a promising alternative in the failure analysis of composite materials, with the consideration of local damage and unguided path in the materials. The constituents of composites can be modelled with different bond models based on DEM. However, the strength of bonds should be calibrated from experiments before conducting a microscale failure analysis due to the

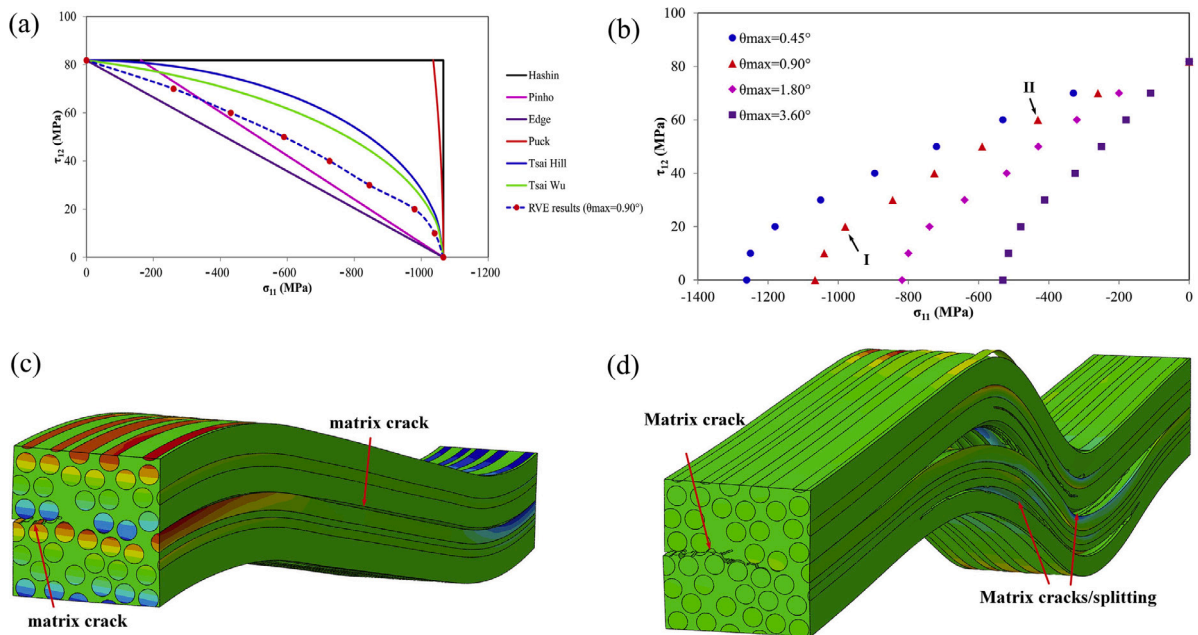


**Fig. 13.** (a) Failure envelopes of  $\sigma_{11} - \tau_{12}$  for different waviness angles  $\theta_{max}$ , (b) and (c) present the failure modes corresponding to the points I and II in (a) for  $\theta_{max} = 0.9^\circ$ , respectively [44]. (Solid lines in (a) represent the failure envelopes predicted by various failure criteria, dash blue line represents the fitted failure envelopes based on the real failure points predicted by numerical simulations in the combined longitudinal compression and in-plane shear. Failure criteria were found to either overestimate or underestimate the failure strength under the biaxial loadings. Different colourful dots represent the failure points under combined longitudinal compression and in-plane shear with different initial waviness angles. The failure strength was found to decrease as the angle increased. (c) and (d) represent the two different failure modes, fibre kinking and matrix cracking/splitting, at different stress states I and II, respectively. (For interpretation of the references to colour in this figure legend, the reader is referred to the web version of this article.)

randomly distributed bonds. In addition, the computational cost is another challenge when using DEM, but can be partially mitigated with GPU acceleration.

The application of computational micromechanical presents great potential to evaluate the mechanical properties and to reveal failure mechanisms as well as the damage propagation process in great detail. Although great efforts have been made in the microscale simulation of FRP composites and fruitful results have been achieved, there still exist some aspects that can be improved:

- The constitutive model of fibre needs to be developed from a physics point of view by considering the nonlinearity of its behaviour and the difference in tensile and compressive loadings, especially in fibre failure-dominated loadings.
- The manufacturing-induced defects, i.e. voids, fibre misalignment etc., should be included in the micromechanical models to capture the characteristics of stochastic phenomena in the progressive failure analysis of composites, especially under multiaxial loadings.
- The in-situ effect of polymer behaviour and the friction between fibre and matrix should be taken into account when constructing the micromechanics models for composites. This enables the numerical simulations closer to the mechanical performance of composites in reality.
- Failure criteria assessment should be conducted based on the failure analysis of FRP composite under more complex multiaxial stress with micromechanics-based modelling, which cannot be realised experimentally currently.
- GPU acceleration should be considered into the DEM modelling to mitigate its computational costs via commercial software or open-source codes.

#### Declaration of competing interest

The authors declare that they have no known competing financial interests or personal relationships that could have appeared to influence the work reported in this paper.

#### Data availability

Data will be made available on request.

#### References

- [1] L. Wan, Progressive Damage Mechanisms and Failure Predictions of Fibre-Reinforced Polymer Composites Under Quasi-Static Loads Using the Finite Element and Discrete Element Methods (Ph.D. thesis), University of Edinburgh, 2020.
- [2] J. Llorca, C. González, J.M. Molina-Aldareguía, J. Segurado, R. Seltzer, F. Sket, M. Rodríguez, S. Sádaba, R. Muñoz, L.P. Canal, Multiscale modeling of composite materials: A roadmap towards virtual testing, *Adv. Mater.* 23 (44) (2011) 5130–5147.
- [3] L. Mishnaevsky, Composite materials for wind energy applications: Micromechanical modeling and future directions, *Comput. Mech.* 50 (2) (2012) 195–207.
- [4] F. Naya, C. González, C.S. Lopes, S.V. der Veen, F. Pons, Computational micromechanics of the transverse and shear behavior of unidirectional fiber reinforced polymers including environmental effects, *Composites A* 92 (2017) 146–157.
- [5] M. Heidari-Rarani, K. Bashandeh-Khodaei-Naeni, S. Mirkhalaf, Micromechanical modeling of the mechanical behavior of unidirectional composites – A comparative study, *J. Reinf. Plast. Compos.* 37 (16) (2018) 1051–1071.
- [6] C. González, J. Llorca, Mechanical behavior of unidirectional fiber-reinforced polymers under transverse compression: Microscopic mechanisms and modeling, *Compos. Sci. Technol.* 67 (13) (2007) 2795–2806.
- [7] A. Sharma, S. Daggumati, A. Gupta, W. Van Paepegem, On the prediction of the bi-axial failure envelope of a UD CFRP composite lamina using computational micromechanics: Effect of microscale parameters on macroscale stress-strain behavior, *Compos. Struct.* 251 (2020) 112605.
- [8] T. Vaughan, C. McCarthy, A combined experimental-numerical approach for generating statistically equivalent fibre distributions for high strength laminated composite materials, *Compos. Sci. Technol.* 70 (2) (2010) 291–297.
- [9] V. Buryachenko, N. Pagano, R. Kim, J. Spowart, Quantitative description and numerical simulation of random microstructures of composites and their effective elastic moduli, *Int. J. Solids Struct.* 40 (1) (2003) 47–72.
- [10] A. Wongsto, S. Li, Micromechanical FE analysis of UD fibre-reinforced composites with fibres distributed at random over the transverse cross-section, *Composites A* 36 (9) (2005) 1246–1266.
- [11] A. Melro, P. Camanho, S. Pinho, Generation of random distribution of fibres in long-fibre reinforced composites, *Compos. Sci. Technol.* 68 (9) (2008) 2092–2102.

- [12] L. Yang, Y. Yan, Z. Ran, Y. Liu, A new method for generating random fibre distributions for fibre reinforced composites, *Compos. Sci. Technol.* 76 (2013) 14–20.
- [13] Y. Ismail, D. Yang, J. Ye, Discrete element method for generating random fibre distributions in micromechanical models of fibre reinforced composite laminates, *Composites B* 90 (2016) 485–492.
- [14] I. Itasca Consulting Group Inc., PFC 5.0 documentation, 2011.
- [15] C. González, J. Llorca, Mechanical behavior of unidirectional fiber-reinforced polymers under transverse compression: Microscopic mechanisms and modeling, *Compos. Sci. Technol.* 67 (13) (2007) 2795–2806.
- [16] W. Tan, F. Naya, L. Yang, T. Chang, B.G. Falzon, L. Zhan, J.M. Molina-Aldareguía, C. González, J. Llorca, The role of interfacial properties on the intralaminar and interlaminar damage behaviour of unidirectional composite laminates: Experimental characterization and multiscale modelling, *Composites B* 138 (2018) 206–221.
- [17] J. Múgica, C. Lopes, F. Naya, M. Herráez, V. Martínez, C. González, Multiscale modelling of thermoplastic woven fabric composites: From micromechanics to mesomechanics, *Compos. Struct.* 228 (2019) 111340.
- [18] W. Weibull, A statistical distribution function of wide applicability, *J. Appl. Mech.* (1951).
- [19] R.P. Tavares, A.R. Melro, M.A. Bessa, A. Turon, W.K. Liu, P.P. Camanho, Mechanics of hybrid polymer composites: Analytical and computational study, *Comput. Mech.* 57 (3) (2016) 405–421.
- [20] L.F. Varandas, G. Catalanotti, A. Melro, R. Tavares, B.G. Falzon, Micromechanical modelling of the longitudinal compressive and tensile failure of unidirectional composites: The effect of fibre misalignment introduced via a stochastic process, *Int. J. Solids Struct.* 203 (2020) 157–176.
- [21] F. Naya, M. Herráez, C. Lopes, C. González, S. Van der Veen, F. Pons, Computational micromechanics of fiber kinking in unidirectional FRP under different environmental conditions, *Compos. Sci. Technol.* 144 (2017) 26–35.
- [22] S. Pimenta, R. Gutkin, S. Pinho, P. Robinson, A micromechanical model for kink-band formation: Part I—Experimental study and numerical modelling, *Compos. Sci. Technol.* 69 (7–8) (2009) 948–955.
- [23] M. Bishara, R. Rolfes, O. Allix, Revealing complex aspects of compressive failure of polymer composites-Part I: Fiber kinking at microscale, *Compos. Struct.* 169 (2017) 105–115.
- [24] L. Zhou, L. Zhao, F. Liu, J. Zhang, A micromechanical model for longitudinal compressive failure in unidirectional fiber reinforced composite, *Results Phys.* 10 (2018) 841–848.
- [25] M. Herráez Matesanz, *Computational Micromechanics Models for Damage and Fracture of Fiber-Reinforced Polymers* (Ph.D. thesis), Caminos, 2018.
- [26] I. Kowalski, Characterizing the Tensile Stress-Strain Nonlinearity of Polyacrylonitrile-Based Carbon Fibers, ASTM International, 1988.
- [27] B. Fiedler, M. Hojo, S. Ochiai, K. Schulte, M. Ando, Failure behavior of an epoxy matrix under different kinds of static loading, *Compos. Sci. Technol.* 61 (11) (2001) 1615–1624.
- [28] D.C. Drucker, W. Prager, Soil mechanics and plastic analysis or limit design, *Quart. Appl. Math.* 10 (2) (1952) 157–165.
- [29] H. Hooputra, H. Gese, H. Dell, H. Werner, A comprehensive failure model for crashworthiness simulation of aluminium extrusions, *Int. J. Crashworthiness* 9 (5) (2004) 449–464.
- [30] Abaqus Users Manual, Version 6.13, 2013, Dassault Systèmes Simulia Corp., Providence, Rhode Island, USA.
- [31] J. Lubliner, J. Oliver, S. Oller, E. Oñate, A plastic-damage model for concrete, *Int. J. Solids Struct.* 25 (3) (1989) 299–326.
- [32] J. Lee, G.L. Fenves, Plastic-damage model for cyclic loading of concrete structures, *J. Eng. Mech.* 124 (8) (1998) 892–900.
- [33] A.R. Melro, P.P. Camanho, F.M.A. Pires, S.T. Pinho, Micromechanical analysis of polymer composites reinforced by unidirectional fibres: Part I – Constitutive modelling, *Int. J. Solids Struct.* 50 (11) (2013) 1897–1905.
- [34] P. Menetrey, K. Willam, Triaxial failure criterion for concrete and its generalization, *Struct. J.* 92 (3) (1995) 311–318.
- [35] H. Subramanya, S. Viswanath, R. Narasimhan, A three-dimensional numerical study of mode I crack tip fields in pressure sensitive plastic solids, *Int. J. Solids Struct.* 44 (6) (2007) 1863–1879.
- [36] Z.P. Bažant, B.H. Oh, Crack band theory for fracture of concrete, *Matériaux Et Construction* 16 (3) (1983) 155–177.
- [37] L. Yang, Y. Yan, Y. Liu, Z. Ran, Microscopic failure mechanisms of fiber-reinforced polymer composites under transverse tension and compression, *Compos. Sci. Technol.* 72 (15) (2012) 1818–1825.
- [38] K. Xu, W. Chen, L. Liu, Z. Zhao, G. Luo, A hierarchical multiscale strategy for analyzing the impact response of 3D braided composites, *Int. J. Mech. Sci.* 193 (2021) 106167.
- [39] N.W. Tschoegl, Failure surfaces in principal stress space, *J. J. Polym. Sci. C: Polym. Symp.* 32 (1) (1971) 239–267.
- [40] H. Koerber, J. Xavier, P.P. Camanho, High strain rate characterisation of unidirectional carbon-epoxy IM7-8552 in transverse compression and in-plane shear using digital image correlation, *Mech. Mater.* 42 (11) (2010) 1004–1019.
- [41] G. Alfano, E. Sacco, Combining interface damage and friction in a cohesive-zone model, *Internat. J. Numer. Methods Engrg.* 68 (5) (2006) 542–582.
- [42] A. Turon, E. González, C. Sarrado, G. Guillaumet, P. Maimí, Accurate simulation of delamination under mixed-mode loading using a cohesive model with a mode-dependent penalty stiffness, *Compos. Struct.* 184 (2018) 506–511.
- [43] A.R. Melro, P.P. Camanho, F.M.A. Pires, S.T. Pinho, Micromechanical analysis of polymer composites reinforced by unidirectional fibres: Part II – Micromechanical analyses, *Int. J. Solids Struct.* 50 (11) (2013) 1906–1915.
- [44] Q. Sun, G. Zhou, Z. Meng, H. Guo, Z. Chen, H. Liu, H. Kang, S. Ketten, X. Su, Failure criteria of unidirectional carbon fiber reinforced polymer composites informed by a computational micromechanics model, *Compos. Sci. Technol.* 172 (2019) 81–95.
- [45] M. Romanowicz, A numerical approach for predicting the failure locus of fiber reinforced composites under combined transverse compression and axial tension, *Comput. Mater. Sci.* 51 (1) (2012) 7–12.
- [46] E. Totry, C. González, J. Llorca, Prediction of the failure locus of C/PEEK composites under transverse compression and longitudinal shear through computational micromechanics, *Compos. Sci. Technol.* 68 (15) (2008) 3128–3136.
- [47] J. Lu, P. Zhu, Q. Ji, Q. Feng, J. He, Identification of the mechanical properties of the carbon fiber and the interphase region based on computational micromechanics and Kriging metamodel, *Comput. Mater. Sci.* 95 (2014) 172–180.
- [48] Y. Ismail, L. Wan, J. Chen, J. Ye, D. Yang, An ABAQUS® plug-in for generating virtual data required for inverse analysis of unidirectional composites using artificial neural networks, *Eng. Comput.* 38 (5) (2022) 4323–4335.
- [49] C. Zhu, P. Zhu, Z. Liu, W. Tao, Numerical investigation of fiber random distribution on the mechanical properties of yarn in-plain woven carbon fiber-reinforced composite based on a new perturbation algorithm, *J. Compos. Mater.* 52 (6) (2018) 755–771.
- [50] J. Chen, L. Wan, Y. Ismail, J. Ye, D. Yang, A micromechanics and machine learning coupled approach for failure prediction of unidirectional CFRP composites under triaxial loading: A preliminary study, *Compos. Struct.* 267 (2021) 113876.
- [51] J. Chen, L. Wan, Y. Ismail, P. Hou, J. Ye, D. Yang, Micromechanical analysis of UD CFRP composite lamina under multiaxial loading with different loading paths, *Compos. Struct.* 269 (2021) 114024.
- [52] M. Benzeggagh, M. Kenane, Measurement of mixed-mode delamination fracture toughness of unidirectional glass/epoxy composites with mixed-mode bending apparatus, *Compos. Sci. Technol.* 56 (4) (1996) 439–449.
- [53] D. O’dwyer, N. O’dowd, C. McCarthy, Numerical micromechanical investigation of interfacial strength parameters in a carbon fibre composite material, *J. Compos. Mater.* 48 (6) (2014) 749–760.
- [54] E. Totry, J.M. Molina-Aldareguía, C. González, J. Llorca, Effect of fiber, matrix and interface properties on the in-plane shear deformation of carbon-fiber reinforced composites, *Compos. Sci. Technol.* 70 (6) (2010) 970–980.
- [55] T. Vaughan, C. McCarthy, Micromechanical modelling of the transverse damage behaviour in fibre reinforced composites, *Compos. Sci. Technol.* 71 (3) (2011) 388–396.
- [56] E. Totry, C. González, J. Llorca, Failure locus of fiber-reinforced composites under transverse compression and out-of-plane shear, *Compos. Sci. Technol.* 68 (3) (2008) 829–839.
- [57] L. Yang, Z. Wu, Y. Cao, Y. Yan, Micromechanical modelling and simulation of unidirectional fibre-reinforced composite under shear loading, *J. Reinf. Plast. Compos.* 34 (1) (2015) 72–83.
- [58] L. Wan, Y. Ismail, C. Zhu, P. Zhu, Y. Sheng, J. Liu, D. Yang, Computational micromechanics-based prediction of the failure of unidirectional composite lamina subjected to transverse and in-plane shear stress states, *J. Compos. Mater.* 54 (24) (2020) 3637–3654.
- [59] T. Sebaey, G. Catalanotti, C. Lopes, N. O’Dowd, Computational micromechanics of the effect of fibre misalignment on the longitudinal compression and shear properties of UD fibre-reinforced plastics, *Compos. Struct.* 248 (2020) 112487.
- [60] M. Herráez, A. Bergan, C. Lopes, C. González, Computational micromechanics model for the analysis of fiber kinking in unidirectional fiber-reinforced polymers, *Mech. Mater.* 142 (2020) 103299.
- [61] N. Tschoegl, Failure surfaces in principal stress space, *J. Polym. Sci. C: Polym. Symp.* 32 (1) (1971) 239–267.
- [62] Q. Sun, Z. Meng, G. Zhou, S.P. Lin, H. Kang, S. Ketten, H. Guo, X. Su, Multi-scale computational analysis of unidirectional carbon fiber reinforced polymer composites under various loading conditions, *Compos. Struct.* 196 (2018) 30–43.
- [63] S. Costa, H. Zrida, R. Olsson, M. Herráez, R. Östlund, A unified physically-based finite deformation model for damage growth in composites, *Composites A* 161 (2022) 107103.
- [64] J. Lu, P. Zhu, Q. Ji, Q. Feng, J. He, Identification of the mechanical properties of the carbon fiber and the interphase region based on computational micromechanics and Kriging metamodel, *Comput. Mater. Sci.* 95 (2014) 172–180.
- [65] C. Zhu, P. Zhu, Z. Liu, W. Tao, Numerical investigation of fiber random distribution on the mechanical properties of yarn in-plain woven carbon fiber-reinforced composite based on a new perturbation algorithm, *J. Compos. Mater.* 52 (6) (2018) 755–771.

- [66] D. Garoz, F. Gilibert, R. Sevenois, S. Spronk, W.V. Paepegem, Consistent application of periodic boundary conditions in implicit and explicit finite element simulations of damage in composites, *Composites B* 168 (2019) 254–266.
- [67] L.E. Asp, L.A. Berglund, R. Talreja, Prediction of matrix-initiated transverse failure in polymer composites, *Compos. Sci. Technol.* 56 (9) (1996) 1089–1097.
- [68] L. Asp, L.A. Berglund, R. Talreja, Effects of fiber and interphase on matrix-initiated transverse failure in polymer composites, *Compos. Sci. Technol.* 56 (6) (1996) 657–665.
- [69] C. Vargel, Chapter b.2 - types of corrosion on aluminium, in: C. Vargel (Ed.), *Corrosion of Aluminium*, 2004, pp. 113–146.
- [70] Y. Huang, K.K. Jin, S.K. Ha, Effects of fiber arrangement on mechanical behavior of unidirectional composites, *J. Compos. Mater.* 42 (18) (2008) 1851–1871.
- [71] J.H. Oh, K.K. Jin, S.K. Ha, Interfacial strain distribution of a unidirectional composite with randomly distributed fibers under transverse loading, *J. Compos. Mater.* 40 (9) (2006) 759–778.
- [72] S.K. Ha, Y. Huang, H.H. Han, K.K. Jin, Micromechanics of failure for ultimate strength predictions of composite laminates, *J. Compos. Mater.* 44 (20) (2010) 2347–2361.
- [73] D. Trias, J. Costa, J.A. Mayugo, J.E. Hurtado, Random models versus periodic models for fibre reinforced composites, *Comput. Mater. Sci.* 38 (2) (2006) 316–324.
- [74] D. Trias, J. Costa, A. Turon, J. Hurtado, Determination of the critical size of a statistical representative volume element (SRVE) for carbon reinforced polymers, *Acta Mater.* 54 (13) (2006) 3471–3484.
- [75] J. Moraleda, J. Segurado, J. Llorca, Effect of interface fracture on the tensile deformation of fiber-reinforced elastomers, *Int. J. Solids Struct.* 46 (25) (2009) 4287–4297.
- [76] Y.-B. Shang, H.-J. Shi, Micromechanical analysis of stochastic fiber/matrix interface strength effect on transverse tensile property of fiber reinforced composites, *J. Reinf. Plast. Compos.* 34 (2) (2015) 131–144.
- [77] F. Paris, E. Correa, J. Cañas, Micromechanical view of failure of the matrix in fibrous composite materials, *Compos. Sci. Technol.* 63 (7) (2003) 1041–1052.
- [78] D. O'Dwyer, N. O'Dowd, C. McCarthy, Investigation of strain hardening effects under in-plane shear of unidirectional composite materials, *Comput. Mater. Sci.* 64 (2012) 179–182.
- [79] T. Vaughan, C. McCarthy, A micromechanical study on the effect of intraply properties on transverse shear fracture in fibre reinforced composites, *Composites A* 42 (9) (2011) 1217–1228.
- [80] S. Blassiau, A. Thionnet, A.R. Bunsell, Micromechanisms of load transfer in a unidirectional carbon fibre-reinforced epoxy composite due to fibre failures. Part 1: Micromechanisms and 3D analysis of load transfer: The elastic case, *Compos. Struct.* 74 (3) (2006) 303–318.
- [81] S. Blassiau, A. Thionnet, A.R. Bunsell, Micromechanisms of load transfer in a unidirectional carbon fibre-reinforced epoxy composite due to fibre failures. Part 2: Influence of viscoelastic and plastic matrices on the mechanisms of load transfer, *Compos. Struct.* 74 (3) (2006) 319–331.
- [82] S. Blassiau, A. Thionnet, A.R. Bunsell, Micromechanisms of load transfer in a unidirectional carbon fibre-reinforced epoxy composite due to fibre failures: Part 3. Multiscale reconstruction of composite behaviour, *Compos. Struct.* 83 (3) (2008) 312–323.
- [83] H.W. Wang, H.W. Zhou, L. Mishnaevsky, P. Brøndsted, L.N. Wang, Single fibre and multifibre unit cell analysis of strength and cracking of unidirectional composites, *Comput. Mater. Sci.* 46 (4) (2009) 810–820.
- [84] L. Mishnaevsky, P. Brøndsted, Three-dimensional numerical modelling of damage initiation in unidirectional fiber-reinforced composites with ductile matrix, *Mater. Sci. Eng. A* 498 (1) (2008) 81–86.
- [85] L. Mishnaevsky, P. Brøndsted, Micromechanisms of damage in unidirectional fiber reinforced composites: 3D computational analysis, *Compos. Sci. Technol.* 69 (7) (2009) 1036–1044.
- [86] F. Naya Montáns, Prediction of Mechanical Properties of Unidirectional FRP Plies at Different Environmental Conditions by Means of Computational Micromechanics (Ph.D. thesis), Caminos, 2017.
- [87] C. Gonzalez, J. Llorca, Multiscale modeling of fracture in fiber-reinforced composites, *Acta Mater.* 54 (16) (2006) 4171–4181.
- [88] S. Kyriakides, R. Arseculeratne, E. Perry, K. Liechti, On the compressive failure of fiber reinforced composites, *Int. J. Solids Struct.* 32 (6–7) (1995) 689–738.
- [89] S.-Y. Hsu, T.J. Vogler, S. Kyriakides, Compressive strength predictions for fiber composites, *J. Appl. Mech.* 65 (1) (1998) 7–16.
- [90] S.-Y. Hsu, T. Vogler, S. Kyriakides, On the axial propagation of kink bands in fiber composites: Part II Analysis, *Int. J. Solids Struct.* 36 (4) (1999) 575–595.
- [91] T. Vogler, S. Kyriakides, On the initiation and growth of kink bands in fiber composites: Part I. Experiments, *Int. J. Solids Struct.* 38 (15) (2001) 2639–2651.
- [92] T. Vogler, S.-Y. Hsu, S. Kyriakides, On the initiation and growth of kink bands in fiber composites. Part II: Analysis, *Int. J. Solids Struct.* 38 (15) (2001) 2653–2682.
- [93] P. Prabhakar, A.M. Waas, Interaction between kinking and splitting in the compressive failure of unidirectional fiber reinforced laminated composites, *Compos. Struct.* 98 (2013) 85–92.
- [94] X. Bai, M.A. Bessa, A.R. Melro, P.P. Camanho, L. Guo, W.K. Liu, High-fidelity micro-scale modeling of the thermo-visco-plastic behavior of carbon fiber polymer matrix composites, *Compos. Struct.* 134 (2015) 132–141.
- [95] P.A. Cundall, A computer model for simulating progressive, large scale movement in blocky rock systems, 1971.
- [96] P.A. Cundall, O.D.L. Strack, A discrete numerical model for granular assemblies, *Geotechnique* 29 (1979) 47–65.
- [97] L. Wan, D. Yang, Y. Ismail, Y. Sheng, 3D particle models for composite laminates with anisotropic elasticity, *Composites B* 149 (2018) 110–121.
- [98] L. Trivino, B. Mohanty, Assessment of crack initiation and propagation in rock from explosion-induced stress waves and gas expansion by cross-hole seismometry and FEM-DEM method, *Int. J. Rock Mech. Min. Sci.* 77 (Supplement C) (2015) 287–299.
- [99] M. Nitka, J. Tejchman, Modelling of concrete behaviour in uniaxial compression and tension with DEM, *Granul. Matter* 17 (1) (2015) 145–164.
- [100] S. Jiang, T. Li, Y. Tan, A DEM methodology for simulating the grinding process of SiC ceramics, *Procedia Eng.* 102 (Supplement C) (2015) 1803–1810.
- [101] D. Yang, J. Ye, Y. Tan, Y. Sheng, Modeling progressive delamination of laminated composites by discrete element method, *Comput. Mater. Sci.* 50 (3) (2011) 858–864.
- [102] V. Mantić, L. Távora, A. Blázquez, E. Graciani, F. París, A linear elastic-brittle interface model: Application for the onset and propagation of a fibre-matrix interface crack under biaxial transverse loads, *Int. J. Fract.* 195 (1) (2015) 15–38.
- [103] L. Wan, Y. Sheng, E.D. McCarthy, D. Yang, A novel approach for 3D discrete element modelling the progressive delamination in unidirectional CFRP composites, *Eng. Fract. Mech.* (2022) 108982.
- [104] S. Lenci, Analysis of a crack at a weak interface, *Int. J. Fract.* 108 (3) (2001) 275–290.
- [105] A. Carpinteri, P. Cornetti, N. Pugno, Edge debonding in FRP strengthened beams: Stress versus energy failure criteria, *Eng. Struct.* 31 (10) (2009) 2436–2447.
- [106] M.-B. Liu, G.-R. Liu, Particle Methods for Multi-Scale and Multi-Physics, World Scientific, 2015.
- [107] L. Wan, Y. Ismail, Y. Sheng, K. Wu, D. Yang, Progressive failure analysis of CFRP composite laminates under uniaxial tension using a discrete element method, *J. Compos. Mater.* 55 (8) (2021) 1091–1108.
- [108] F.A. Tavarez, M.E. Plesha, Discrete element method for modelling solid and particulate materials, *Internat. J. Numer. Methods Engrg.* 70 (4) (2007) 379–404.
- [109] C. Liu, D.D. Pollard, B. Shi, Analytical solutions and numerical tests of elastic and failure behaviors of close-packed lattice for brittle rocks and crystals, *J. Geophys. Res.: Solid Earth* 118 (1) (2013) 71–82.
- [110] G.-F. Zhao, J. Fang, J. Zhao, A 3D distinct lattice spring model for elasticity and dynamic failure, *Int. J. Numer. Anal. Methods Geomech.* 35 (8) (2011) 859–885.
- [111] L. Maheo, F. Dau, D. André, J.L. Charles, I. Iordanoff, A promising way to model cracks in composite using discrete element method, *Composites B* 71 (2015) 193–202.
- [112] Y. Ismail, D. Yang, J. Ye, Discrete element method for generating random fibre distributions in micromechanical models of fibre reinforced composite laminates, *Composites B* 90 (2016) 485–492.
- [113] Y. Ismail, Y. Sheng, D. Yang, J. Ye, Discrete element modelling of unidirectional fibre-reinforced polymers under transverse tension, *Composites B* 73 (2015) 118–125.
- [114] Y. Ismail, D. Yang, J. Ye, A DEM model for visualising damage evolution and predicting failure envelope of composite laminae under biaxial loads, *Composites B* 102 (2016) 9–28.
- [115] Y. Sheng, D. Yang, Y. Tan, J. Ye, Microstructure effects on transverse cracking in composite laminae by DEM, *Compos. Sci. Technol.* 70 (14) (2010) 2093–2101.
- [116] X. Ding, X. Hou, M. Xia, Y. Ismail, J. Ye, Predictions of macroscopic mechanical properties and microscopic cracks of unidirectional fibre-reinforced polymer composites using deep neural network (DNN), *Compos. Struct.* (2022) 116248.
- [117] P.F. Liu, J.Y. Zheng, Recent developments on damage modeling and finite element analysis for composite laminates: A review, *Mater. Des.* 31 (8) (2010) 3825–3834.
- [118] L.J. Hart-Smith, Predictions of the original and truncated maximum-strain failure models for certain fibrous composite laminates, *Compos. Sci. Technol.* 58 (7) (1998) 1151–1178.
- [119] W.E. Wolfe, T.S. Butalia, A strain-energy based failure criterion for non-linear analysis of composite laminates subjected to biaxial loading, *Compos. Sci. Technol.* 58 (7) (1998) 1107–1124.
- [120] R.M. Christensen, Stress based yield/failure criteria for fiber composites, *Int. J. Solids Struct.* 34 (5) (1997) 529–543.
- [121] W.C. Cui, M.R. Wisnom, A combined stress-based and fracture-mechanics-based model for predicting delamination in composites, *Composites* 24 (6) (1993) 467–474.
- [122] J.M. Whitney, R.J. Nuismer, Stress fracture criteria for laminated composites containing stress concentrations, *J. Compos. Mater.* 8 (3) (1974) 253–265.
- [123] C.T. Sun, J. Tao, Prediction of failure envelopes and stress/strain behaviour of composite laminates, *Compos. Sci. Technol.* 58 (7) (1998) 1125–1136.

- [124] S.W. Tsai, E.M. Wu, A general theory of strength for anisotropic materials, *J. Compos. Mater.* 5 (1) (1971) 58–80.
- [125] O. Hoffman, The brittle strength of orthotropic materials, *J. Compos. Mater.* 1 (2) (1967) 200–206.
- [126] Z. Hashin, Failure criteria for unidirectional fiber composites, *J. Appl. Mech.* 47 (2) (1980) 329–334.
- [127] A. Puck, H. Schürmann, Failure analysis of FRP laminates by means of physically based phenomenological models, *Compos. Sci. Technol.* 62 (12) (2002) 1633–1662.
- [128] S.T. Pinho, L. Iannucci, P. Robinson, Physically-based failure models and criteria for laminated fibre-reinforced composites with emphasis on fibre kinking: Part I: Development, *Composites A* 37 (1) (2006) 63–73.
- [129] C.G. Davila, P.P. Camanho, C.A. Rose, Failure criteria for FRP laminates, *J. Compos. Mater.* 39 (4) (2005) 323–345.
- [130] R. Gutkin, S. Pinho, P. Robinson, P. Curtis, Micro-mechanical modelling of shear-driven fibre compressive failure and of fibre kinking for failure envelope generation in CFRP laminates, *Compos. Sci. Technol.* 70 (8) (2010) 1214–1222.
- [131] A.S. Kaddour, M.J. Hinton, Maturity of 3D failure criteria for fibre-reinforced composites: Comparison between theories and experiments: Part B of WWFE-II, *J. Compos. Mater.* 47 (6–7) (2013) 925–966.
- [132] A.S. Kaddour, M.J. Hinton, P.A. Smith, S. Li, A comparison between the predictive capability of matrix cracking, damage and failure criteria for fibre reinforced composite laminates: Part A of the third world-wide failure exercise, *J. Compos. Mater.* 47 (20–21) (2013) 2749–2779.
- [133] P.D. Soden, A.S. Kaddour, M.J. Hinton, Recommendations for designers and researchers resulting from the world-wide failure exercise, *Compos. Sci. Technol.* 64 (3) (2004) 589–604.
- [134] M.J. Hinton, P.D. Soden, Predicting failure in composite laminates: The background to the exercise, *Compos. Sci. Technol.* 58 (7) (1998) 1001–1010.
- [135] M.J. Hinton, A.S. Kaddour, P.D. Soden, Evaluation of failure prediction in composite laminates: Background to 'Part C' of the exercise, *Compos. Sci. Technol.* 64 (3) (2004) 321–327.
- [136] R.M. Christensen, The world wide failure exercise II examination of results, *J. Reinf. Plast. Compos.* 32 (21) (2013) 1668–1672.
- [137] A.S. Kaddour, M.J. Hinton, P.A. Smith, S. Li, Mechanical properties and details of composite laminates for the test cases used in the third world-wide failure exercise, *J. Compos. Mater.* 47 (20–21) (2013) 2427–2442.
- [138] A.S. Kaddour, M.J. Hinton, P.A. Smith, S. Li, The background to the third world-wide failure exercise, *J. Compos. Mater.* 47 (20–21) (2013) 2417–2426.
- [139] L.P. Canal, J. Segurado, J. LLorca, Failure surface of epoxy-modified fiber-reinforced composites under transverse tension and out-of-plane shear, *Int. J. Solids Struct.* 46 (11) (2009) 2265–2274.
- [140] P. Jelf, N. Fleck, The failure of composite tubes due to combined compression and torsion, *J. Mater. Sci.* 29 (11) (1994) 3080–3084.
- [141] S. Pinho, R. Darvizeh, P. Robinson, C. Schuecker, P. Camanho, Material and structural response of polymer-matrix fibre-reinforced composites, *J. Compos. Mater.* 46 (19–20) (2012) 2313–2341.
- [142] I.M. Daniel, Yield and failure criteria for composite materials under static and dynamic loading, *Prog. Aerosp. Sci.* 81 (2016) 18–25.
- [143] I.M. Daniel, S.M. Daniel, J.S. Fenner, A new yield and failure theory for composite materials under static and dynamic loading, *Int. J. Solids Struct.* 148 (2018) 79–93.
- [144] J. Ye, Y. Wang, Z. Li, M. Saafi, F. Jia, B. Huang, J. Ye, Failure analysis of fiber-reinforced composites subjected to coupled thermo-mechanical loading, *Compos. Struct.* 235 (2020) 111756.
- [145] J. Aboudi, The effect of anisotropic damage evolution on the behavior of ductile and brittle matrix composites, *Int. J. Solids Struct.* 48 (14–15) (2011) 2102–2119.
- [146] E. Massarwa, J. Aboudi, R. Haj-Ali, A multiscale progressive damage analysis for laminated composite structures using the parametric HFGMC micromechanics, *Compos. Struct.* 188 (2018) 159–172.
- [147] H. Khatam, M.-J. Pindera, Parametric finite-volume micromechanics of periodic materials with elastoplastic phases, *Int. J. Plast.* 25 (7) (2009) 1386–1411.
- [148] J. Ye, Y. Hong, L. Liu, H. Cai, W. He, B. Huang, M. Saafi, Y. Wang, J. Ye, Microscale damage evolutions in fiber-reinforced composites with different initial defects, *Compos. Struct.* 279 (2022) 114856.